UNIVERSIDADE FEDERAL DO AMAZONAS
PRÓ-REITORIA DE PESQUISA
PROGRAMA DE PÓS-GRADUAÇÃO EM FÍSICA

YAN MATHEUS COLARES PINTO

INFLUENCE OF DOPING ON SUPERCONDUCTING STATES OF SINGLE-LAYER GRAPHENE .

Manaus-AM
2021

YAN MATHEUS COLARES PINTO

INFLUENCE OF DOPING ON SUPERCONDUCTING STATES OF SINGLE-LAYER GRAPHENE .

Dissertation to be presented as a requirement for obtaining a Master's Degree in Physics, from the Graduate Program in Physics at the Federal University of Amazonas.

Advisor :Prof[a] Dr[a]. Angsula Ghosh

Manaus AM, Brasil
2021

Ficha Catalográfica

Ficha catalográfica elaborada automaticamente de acordo com os dados fornecidos pelo(a) autor(a).

Pinto, Yan Matheus Colares
P659i Influence of doping on superconducting states of single-layer graphene. / Yan Matheus Colares Pinto . 2021
67 f.: il. color; 31 cm.

Orientadora: Angsula Ghosh
Dissertação (Mestrado em Física) - Universidade Federal do Amazonas.

1. Graphene. 2. Superconductivity. 3. Order parameter. 4. Doping. I. Ghosh, Angsula. II. Universidade Federal do Amazonas III. Título

YANMATHEUS COLARES PINTO

Influence of Doping on Superconducting States of Single-layer Graphene.

Dissertação apresentada ao Programa de Pós-Graduação em Física da Universidade Federal do Amazonas, como parte dos requisitos parciais para obtenção do título de Mestre em Física, área de concentração em Física da Matéria Condensada.

Aprovada em 07 de Junho de 2021.

BANCA EXAMINADORA

Profª. Dra. Angsula Ghosh, Presidente
Universidade Federal do Amazonas (UFAM)

Prof. Dr. Ernesto Govea Alcaide, Membro
Universidade Federal do Amazonas (UFAM)

Prof. Dr. Fábio Teixeira Dias, Membro
Universidade Federal de Pelotas (UFPel)

DEDICATION

To my family.

ACKNOWLEDGMENTS

I would like to thank my advisor, Professor Angsula Ghosh, for guiding me during the last two years in PPGFIS and for her incentives me in my studies and research. I also am indebted to Prof. Daniela Menegon, Prof. Ernesto Govea, Prof. Hidemberg Frota and Prof. Fidel Zayas for providing me guidance during my course work, writing and development of my research work. To my colleagues Phillippe, Noah and Raul for their valuable conversations and help. I show my gratitude to the graduate program of Physics of the Federal University of Amazonas as a whole. The author acknowledges the financial support from the Brazilian funding agency Coordenação de Aperfeiçoamento de Pessoal de Nível Superior (CAPES) for the fellowship and also the support during the masters program.

To all my family , in particular: My father, for guiding me to always follow this path. My mother, (Concilei) and sisters (Yasmin and Nicléa), for taking care of me when I needed it. My brother Yago, for the conversations and distractions and my brother Yon for having guided me on my way to the master's test. My partner (Jackeline Maciel) for being with me and for helping me with her great knowledge.

RESUMO

A ascensão de estudos que abordam o grafeno tem sido notável nas últimas décadas, tanto por suas estrutura bidimensional quanto para diversas aplicações em potenciais tecnológicos. Em adição, descobertas sobre fenômenos supercondutores emergem cada vez mais nos diversos materiais quando postos a baixa temperatura, com isso este trabalho tem como enfoque principal o estudo das fases do estado supercondutor na estrutura de rede favo de mel do grafeno.

Para isso, foi fundamentalmente apresentado o grafeno puro por aproximação tight-binding dos elétrons e suas as bandas de energia na primeira zona de Brillouin descrito pela dispersão linear dos férmions de Dirac. Em seguida abordou-se a teoria da supercondutividade através da teoria de campo médio e energias de excitação.

Conciliando esse estado da matéria aplicado ao grafeno e considerando efeitos de dopagem nós analisamos os estados de fase para energias atrativas de interação elétron-elétron.

Obtivemos além da usual onda s, uma exótica possibilidade, uma onda $p + ip$ simétrica devido a estrutura de simetria em torno dos pontos de Dirac e portanto uma coexistência das fases e são obtidos gráficos caracerísticos do parâmetro de ordem e do calor específico com relação a temperatura na variação do potencial químico.

Palavras-chave: Grafeno. Supercondutividade. Parâmetro de ordem.

ABSTRACT

An increase in the number of studies involving graphene has been notable in the recent decades, mainly due its two-dimensional structure and also for the varied applications in technological devices. Superconductivity has been observed in different materials when placed under very-low temperatures, which motivated us to the study the different phases of the superconducting states in the honeycomb lattice structure of graphene.

In this work we consider pure two-dimensional single-layer graphene on a honeycomb lattice. A tight-binding model of the electrons and their energy bands in the first Brillouin zone described by the linear dispersion of the Dirac fermions is used to describe the graphene in its pure form. We study the superconducting phases of the graphene using a mean field theory to calculate the temperature dependencies of the order parameters and also the specific heat of the system below the critical temperature.

Conciling this states of matter applied to graphene and considering doping effects we analized the phases states for attractive electron-electron interactions energies.

We get in addition to the usual s-wave, an exotic possibility appears in the form of a symmetric $p+ip$ wave due to the symmetry structure around the Dirac points. The coexistence of the above two phases has been of utmost importance for our study. Hence the characteristic graphs of the order parameter and specific heat in the variation of the chemical potential are studied.

Keywords: Graphene. Superconductivity. Order parameter.

List of Figures

Summary

Chapter 1

Introduction

Graphene is one of the allotropes of carbon which has a two-dimensional structure, with its atoms organized on a honeycomb lattice. The above structure leads to some interesting and unusual physical properties. Extraordinary electrical and thermal conductivities and very high mechanical strength make graphene a promising candidate for a host of technological applications [5].

The peculiar electronic behavior in Graphene envisages advances in technological applications of great interest for e.g. in electronic sensor bases , LEDs, solar cells, photodetectors, transistors that operate on radio frequency, among others [14] [15]. Evidence of superconductivity in graphene has also attracted a lot of attention in the condensed matter community. The superconducting state in general is induced in graphene by proximity effects with superconducting contacts or by doping. Hence, the presence of superconductivity also confirms the presence of the Cooper pairs that can propagate coherently in graphene. However, there are motivations to make it an intrinsic superconducting material [16]. Experimental and theoretical researchers use the method of intercalated materials, alkali metals in the pure form of graphene at low temperature by chemical modification and by polarizing semiconductor substrates such as Si, Sn, Pb to induce cooper pairs in graphene [12]. For this reason, in this work, we consider we consider superconductivity in graphene and study the cases in which the chemical potential is non-zero representing possible doping in pure graphene.

A study of spin singlet states was developed, with the emergence of the exotic state of the $p+ip$ wave phase which in general is unusual. However, the above state was shown to belong to the structure itself. It was also considered that the energies of the electron-electron interaction potentials of the s and $p+ip$ waves have a value whose module depends on temperature due to their relations with the self-consistent equations.

In this work, we study the temperature dependencies of the order parameters with various values of the interaction parameters. The dependence of the chemical potential of the system on critical temperature and the order parameters were also studied. The normalized gap parameters for the two order parameters also demonstrate a universal nature for all values of the interaction strengths. Moreover, specific heat C_{es} vs temperature for various chemical potential

values demonstrates a consonance with the experimental obtained results with doping.

This present dissertation is organized as follows:

In Chapter 2 we discuss the electronic structure of graphene. The arrangement of the carbon atoms in the crystal lattice and also the interaction of these atoms in the hybridization of orbitals of sp^2 type were considered. The tight-binding model of the graphene single-layer Hamiltonian is discussed in great detail to obtain the dispersion relations of the system.

In chapter 3, a historical overview of superconductivity is presented at the beginning. An explanation of the theory of superconductivity with an emphasis on Cooper pairs, gap energies and order parameter are discussed to provide an understanding of the phenomenon. We also define the thermodynamic quantities of interest related to the excitation energies of the fermions along with their temperature dependencies.

In chapter 4 we discuss the model Hamiltonian considered in our work to study superconductivity in single-layer, pure graphene. The on-site and the nearest neighbor electron-electron interactions are considered to define the superconducting states of graphene. The superconducting order parameters for spin singlet symmetries are defined within a mean-field scenario and are calculated numerically by minimizing the free energy of the system. Specific heat of the superconducting states of graphene in the coexistence phase has also been calculated to study the temperature and doping dependencies of the parameter.

Finally, a short conclusion is presented in chapter 5 with a brief discussion on the future perspectives of the work.

Chapter 2

The Graphene

Graphene can be defined as a single-layer form of graphite. It is a two-dimensional material with honeycomb structure whose structure generates a variety of peculiarities that are reflected in the physical properties,such as its malleability and thermal capacity, high electrical mobility, current conduction capacity, good mechanical resistance, etc.

2.1 Historical Overview.

The twentieth century(XX) was historically remarkable in the development of techniques for understanding the elementary structure of materials. The understanding of the highly layered structure of thermally reduced graphite oxide in the nineteenth century by English chemist Benjamin Collins Brodie paved the way for wondrous discoveries in material science. The advent of the powder-diffraction methods and the formulation of Bragg diffraction and Laue diffraction applied to crystalline solids in 1924 by J.D.Bernal paved new paths [17]. In order to develop a theory for the electronic properties of bulk graphite, physicist Philip Russel Wallace on behalf of National Research Council of Canada directed his attention to explore the material by publishing in 1947 the article entitled "The Band Theory of Graphite" and showed the unusual semimetallic behavior in this material, see Fig. (2.1) . The theory of the structure of the electronic energy bands and Brillouin zones for graphite was developed using the tight binding approximation where along with the overlap of the hexagonal layers of graphite, a single-layer (called Graphene, a term originally introduced years later by H.P. Boemh) was also considered so as to neglect the interaction of the superposition of the planes. A large anisotropy in the electrical conductivity and the diamagnetic susceptibility was exhibited. The work also showed the linear dispersion relation.

It is important to remember that graphene's history spans over more than a century of chemical research. There is a vast chemical literature, literally hundreds of papers during the second half of the twentieth century. Studies on ultra-fine Graphite compounds using TEM (Transmission Electron Microscopic), epitaxial graphite on solid substrates (TiC, TaC, Ni) or chemical exfoliation were performed to understand the layered structure of the graphite. How-

The Band Theory of Graphite

P. R. WALLACE*
National Research Council of Canada, Chalk River Laboratory, Chalk River, Ontario
(Received December 19, 1946)

The structure of the electronic energy bands and Brillouin zones for graphite is developed using the "tight binding" approximation. Graphite is found to be a semi-conductor with zero activation energy, i.e., there are no free electrons at zero temperature, but they are created at higher temperatures by excitation to a band contiguous to the highest one which is normally filled. The electrical conductivity is treated with assumptions about the mean free path. It is found to be about 100 times as great parallel to as across crystal planes. A large and anisotropic diamagnetic susceptibility is predicted for the conduction electrons; this is greatest for fields across the layers. The volume optical absorption is accounted for.

Figure 2.1: P.R.Wallace's article named "The Band of Graphite" published in Physical Review Volume 37 Number 9 on May 1, 1947 [1] .

ever, success only came in 2004 with Andre Geim, Konstantin Novoselov, SV Morozov and his collaborators in the department of the Institute of Microelectronic Technology at the University of Manchester, when graphene was isolated by a direct method of mechanical exfoliation and characterized for the first time utilizing the 'Scotch Tape' method [18]. Hence, when one uses a pencil against a sheet of paper one might be actually producing graphene stacks and among them the presence of the individual graphene layers are highly probable. The number of academic publications regarding the use of graphene continue to grow along the years. Hence, with such an enormous interest in graphene it is imperative for us to study the graphene in more details.

Currently, new approaches are being developed which are not only cost-efficient but also provides secured and environmental friendly solutions to the society. At the National Institute of Technology in India, researcher Vishnu Shanker used eucalyptus bark to extract and synthesize graphene sheets [19]. The CVD (chemical vapor deposition) method, Hummer method and liquid phase exfoliation using extracts of medicinal plants in water were presented by Bipinchandra K. Salunke and Beom Soo Kim [20]. In addition, recently, researchers from the São Carlos Institute of Physics developed a cleaner and faster method to produce reduced graphene using laser-based methods [21].

The application of graphene can be observed in a range of different technologies which could potentially be created and provide some of the many real-world benefits of graphene research [22]. One of the first proposed real-world applications of graphene is related to the high conductivity of graphene and would be ideal for high-speed electronics [23]. Ultra-thin graphene transistors have been developed and could appear in consumer electronics within the next decade. Reducing the size of data storage devices and thereby increasing the capacity of data storage devices whilst maintaining the size is an area which is being considered [24]. Several attempts of producing graphene-based supercapacitors are also being considered to create such technologies [25]. Photovoltaic cells, or solar cells, are also considered to be a potential appli-

cation of graphene [26]. Moreover, another application of graphene can be found in the field of electroanalysis [27]. The electrothermal conduction properties in the production of transistors that operate at low temperatures and at radio frequencies were studied to achieve cut-off frequencies of 155 Gigahertz of the graphene transistor at short wavelengths [14]. Biomolecules, nanoparticles and surfaces in Graphene compounds for Biosensors are capable of recognizing antibodies and organic compounds [15].

Hence, we observe that pure graphene and graphene in compounds could play fundamental roles in the advancement of scientific knowledge which many call it as "The material of the future" owing it to the diversity of its application in the real-world.

2.2 Carbon and its allotropes.

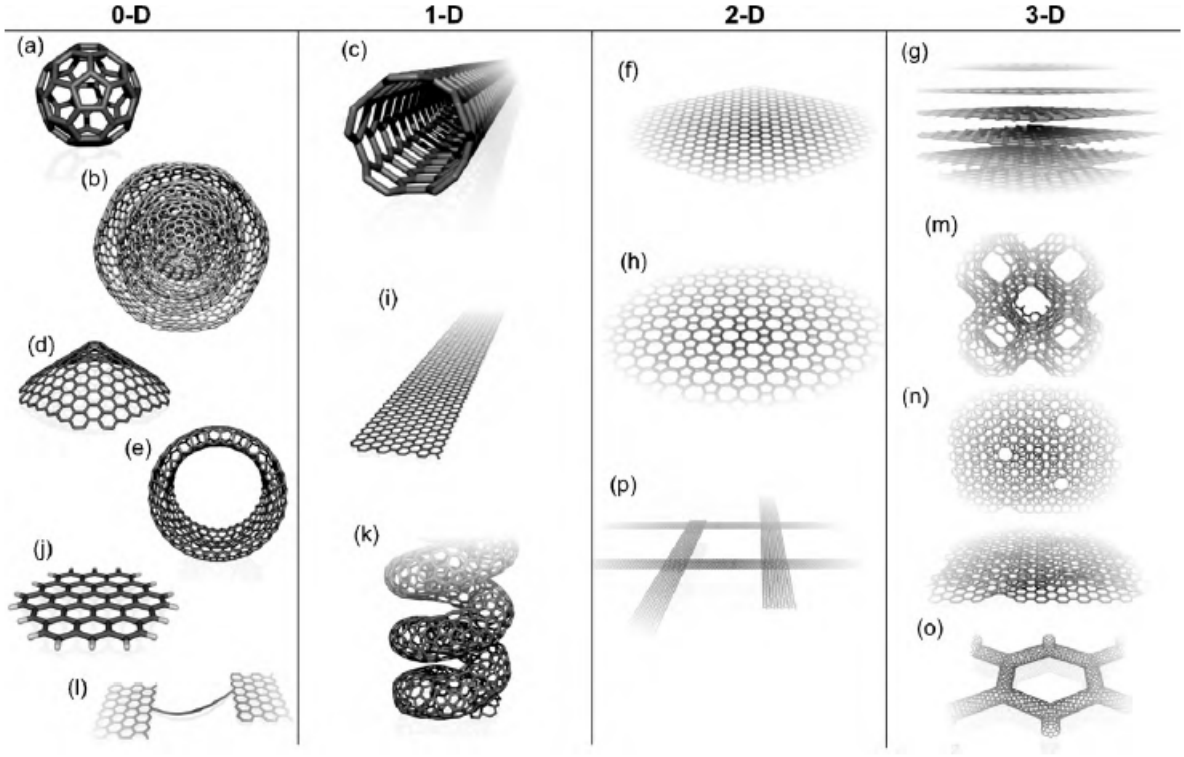

Figure 2.2: Different structures arranged by carbon atoms in different dimensions. a) Buckminsterfulereno. b) Closed fullerene, nested or graphite rings. c) Carbon nanotubes. d) Nanocones. e) Nanothoroids. f) Graphene Honeycomb Structure.g) 3D Graphite Crystal. h) Haeckelite structure. i) Graphene nanofibers. j) Graphene Cluster. k) Helical Carbon Nanotube.l) Small chains of graphene. m) 3D Schwartize crystal. n) Graphene nanostructured foam. o) 3D lattice composed of nanotubes.p) Network of 2D nanofibers [2].

The main constituent carbon of Graphene, a chemical element with atomic number 6, nonmetallic and tetravalent, is a very abundant atom, responsible for the bonding of organic

compounds, minerals and hydrocarbons. It is also called the *materia prima* for life on this planet and the basis of all organic chemistry [2]. It allows us to connect with other substances or even in the form of carbon chains giving rise to various allotropic forms, such as diamond, graphite and many more.

Among the two-dimensional structures demontrated in the figure we observe Graphene in (2.2)(f) where the carbon atoms are organized in the form of a thin layer of carbon. It is the basis for the understanding of the electronic properties in other allotropes. On the other hand, Graphite in (2.2)(g) is the most stable allotrope of Carbon formed from various layers of the graphene sheets and thereby comprising a three-dimensional (3D) crystal.

2.3 Crystalline structure

Carbon is the sixth element in the periodic table and has 6 electrons orbiting around the nucleus in its fundamental state. According to the Pauling Diagram these electrons are arranged in atomic orbitals in the form: 1s, $2s^2$ and $2p^2$. The spatial distribution of the s and p orbitals are illustrated in Fig. (2.3) .

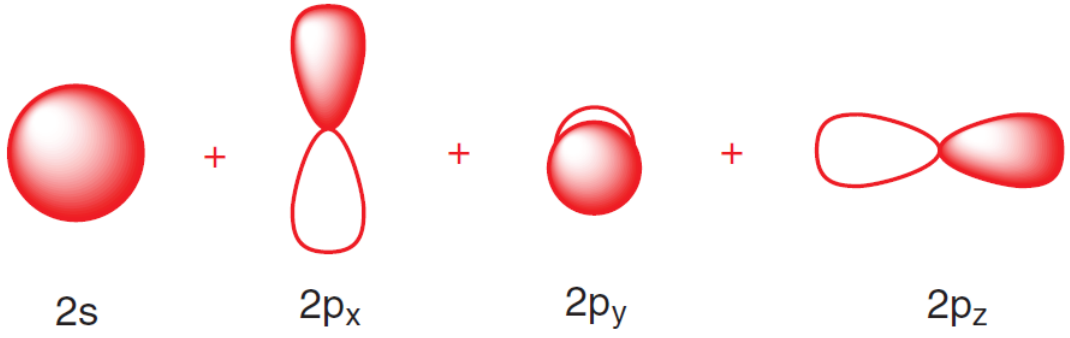

Figure 2.3: s and p orbitals o graphene [3].

The electrons of the symmetric orbitals are in the energy level of quantum number n = 1 and n = 2. The electrons in 1s orbital represent the most strongly connected ones, whereas, the two electrons in 2s are in the outermost shell, n = 2. The electrons in 2p (with possibilities of alignment in the three directions (x, y and z)) are in the valence shell and indicate a possible mixtures of orbitals among them, see Fig. (2.4).

In the case of graphene, hybridization takes place exactly between the 2s, $2p_x$ and $2p_y$ orbitals generating a coplanar and symmetrical 120^o orbital of the type sp^2 forming the σ bonds. The remaining $2p_z$ orbital remains perpendicular to the plane forming weaker π type bonds containing the free electrons participating directly in the conduction of the material. The representation of the above type of bondings are given in Fig. (2.5).

The wave functions of the hybrid orbitals are given in terms of the s and p orbitals and can

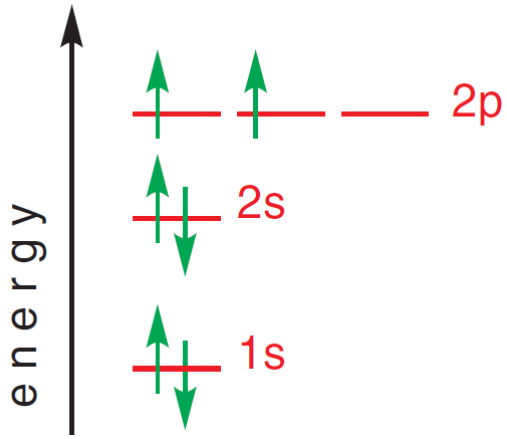

Figure 2.4: Diagram of the fundamental state of carbon [3].

be written as follows:

$$|\psi_1\rangle = \frac{1}{\sqrt{3}}(|s\rangle + |p_x\rangle + |p_y\rangle), \tag{2.1a}$$

$$|\psi_2\rangle = \frac{1}{\sqrt{6}}(|s\rangle + |p_x\rangle - 2\,|p_y\rangle) \tag{2.1b}$$

$$|\psi_3\rangle = \frac{1}{\sqrt{2}}(|s\rangle - |p_x\rangle) \tag{2.1c}$$

In Fig. (2.6) we see the form of the crystalline lattice of graphene (the colored dots represent

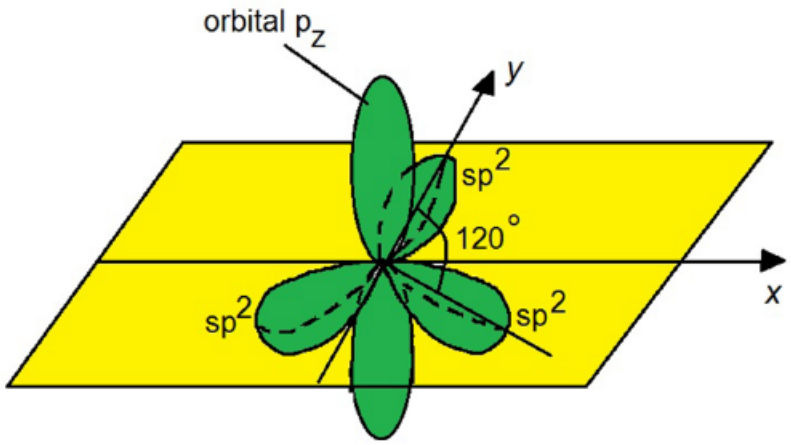

Figure 2.5: The orbitals p_z and sp^2 represented in green. The hybridization orbitals form angles of 120° to each other in the plane (illustrated by the yellow color) x, y and are orthogonal to p_z [4].

the carbon atoms). Graphene is a one-atom-thick layer of carbon atoms arranged in a hexagonal lattice. It and can be visualized as composed of benzene rings stripped out from their hydrogen atoms. The structure of atoms does not form a Bravais lattice as required. In this case the points are seen from their adjacent neighbors, only when rotated through an angle of 180°. Hence, two

triangular sublattices (highlighted in yellow and blue) are considered. The primitive vectors ($\vec{a}_1$ and $\vec{a}_2$) and the relative vectors ($\vec{\delta}_1$, $\vec{\delta}_2$, $\vec{\delta}_3$) on a diatomic basis are defined to obtain a symmetrical Bravais lattice in triangular forms. Therefore, the carbon-carbon distance is given by $a \simeq 1.42 \times 10^{-10} m$ [5]. The primitive vectors are

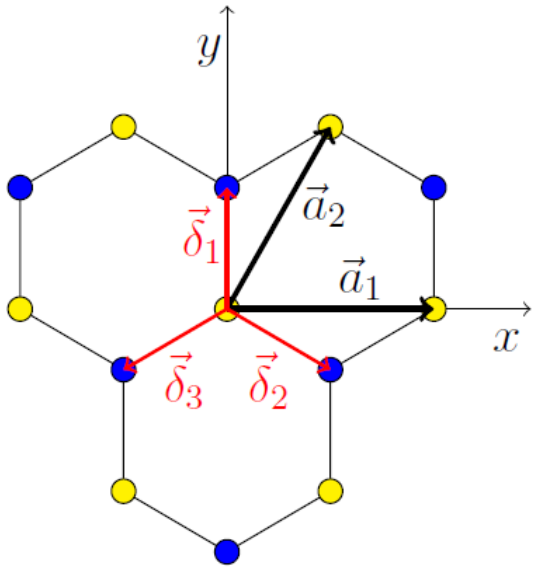

Figure 2.6: Graphene honeycomb structure. The small circles with yellow colors represent sublattice A and the blue ones represent sublattice B. We have the primitive vectors $\vec{a}_1$ and $\vec{a}_2$ and the relative vectors $\vec{\delta}_1$,$\vec{\delta}_2$ e $\vec{\delta}_3$.

$$\vec{a}_1 = \sqrt{3}a\hat{x} + 0\hat{y} + 0\hat{z} \tag{2.2a}$$

$$\vec{a}_2 = \frac{\sqrt{3}a}{2}\hat{x} + \frac{3}{2}\hat{y} + 0\hat{z} \tag{2.2b}$$

where $\hat{x}$, $\hat{y}$ e $\hat{z}$ are unit vectors. The translational vector is given by $\vec{R}$

$$\vec{R} = n\vec{a}_1 + m\vec{a}_2$$

where n and m are integers. The relative vectors are given by:

$$\vec{\delta}_1 = (0, a) \tag{2.3a}$$

$$\vec{\delta}_2 = \left(\frac{a\sqrt{3}}{2}, \frac{a}{2}\right) \tag{2.3b}$$

$$\vec{\delta}_3 = \left(-\frac{a\sqrt{3}}{2}, -\frac{a}{2}\right) \tag{2.3c}$$

In the reciprocal space, the Fourier transformed space of graphene is defined by $\vec{b}_1$, $\vec{b}_2$ and $\vec{b}_1$,

which are given by the following equations:

$$\vec{b}_1 = \left(\frac{2\pi\sqrt{3}}{3a}, -\frac{2\pi}{3a}\right) \tag{2.4a}$$

$$\vec{b}_2 = \left(0, \frac{4\pi}{3a}\right) \tag{2.4b}$$

$$\vec{b}_3 = (0, 0) \tag{2.4c}$$

The reciprocal space is shown in Fig. 2.7. And, just like real space, in reciprocal space we can

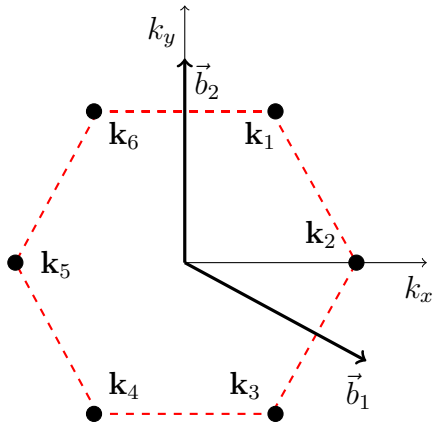

Figure 2.7: (Primitive Wigner-Seitz cell in the reciprocal lattice).

build the entire lattice from the primitive vectors

$$\mathbf{k}_{pq} = p\vec{b}_1 + q\vec{b}_2$$

where the set (p, q) are integers. Now, in the reciprocal space let us analyze the geometric plane formed by the points $(\mathbf{k}_1, \mathbf{k}_2, \mathbf{k}_3, \mathbf{k}_4, \mathbf{k}_5, \mathbf{k}_6)$ which can be identified as the symmetrical points in the reciprocal lattice called Dirac points, which form the primitive cell called Wigner-Seitz Cell. The red dashed line demonstrates the 1st Brillouin zone.

2.4 Tight-Binding model for Graphene.

In order to understand the electronic structure of graphene, we consider the tight-binding Hamiltonian considering the nearest-neighbor hopping and also the next-nearest neighbor hopping parameters [4]. The Hamiltonian is then written as: (see appendix A.7)
(Here we use units that $\hbar = 1$).

$$\hat{H} = -t \sum_{<ij>} \sum_{\sigma} \left(\hat{a}^{\dagger}_{i\sigma}\hat{b}_{j\sigma} + H.c.\right) - t' \sum_{\langle\langle ij\rangle\rangle} \sum_{\sigma} \left(\hat{a}^{\dagger}_{i\sigma}\hat{a}_{j\sigma} + \hat{b}_{i\sigma}\hat{b}^{\dagger}_{j\sigma} + H.c.\right) \tag{2.5}$$

where, t represents the nearest neighbor hopping parameter, $t^{'}$ is the next-nearest hopping parameter, $a^{\dagger}_{i\sigma}, \hat{a}_{i\sigma}$ are the creation and destruction operators in sublattice A whereas $\hat{b}^{\dagger}_{i\sigma}, b_{i\sigma}$ are those in sublattice B. $i(j)$ labels the sites in sublattice $A(B)$ and σ is the spin. It is important to state that $t \cong 2.8$eV and 0.02 eV $\lesssim t^{'} \lesssim$0.2eV [28].

The magnitude of the hopping parameter between the second neighbors is less than 0.1eV [29]. Hence, it can be neglected when compared to t. Therefore, the next-nearest interactions will not be considered in our following discussion. In order to understand the tight-binding model of Hamiltonian, we can write the operators in the momentum space. The Fourier transforms for the creation and annihilation operators are given by:

$$\hat{a}_{i\sigma} = \frac{1}{\sqrt{N}} \sum_{\mathbf{k}} \hat{a}_{\mathbf{k}\sigma} e^{i\mathbf{k}\cdot\vec{r}_i} \tag{2.6a}$$

$$\hat{a}^{\dagger}_{i\sigma} = \frac{1}{\sqrt{N}} \sum_{\mathbf{k}} \hat{a}^{\dagger}_{\mathbf{k}\sigma} e^{-i\mathbf{k}\cdot\vec{r}_i} \tag{2.6b}$$

$$\hat{b}_{j\sigma} = \frac{1}{\sqrt{N}} \sum_{\mathbf{k}} \hat{b}_{\mathbf{k}'\sigma} e^{i\mathbf{k}\cdot\vec{r}_i} \tag{2.6c}$$

$$\hat{b}^{\dagger}_{j\sigma} = \frac{1}{\sqrt{N}} \sum_{\mathbf{k}} \hat{b}^{\dagger}_{\mathbf{k}\sigma} e^{-i\mathbf{k}'\cdot\vec{r}_i} \tag{2.6d}$$

Substituting the above relations in Hamiltonian (2.5) we get:

$$\begin{aligned} \hat{H} \;=\; & -t \sum_{<ij>,\sigma} \left[\left(\frac{1}{\sqrt{N}} \sum_{\mathbf{k}} \hat{a}^{\dagger}_{\mathbf{k}\sigma} e^{-i\mathbf{k}\cdot\vec{r}_i} \right) \left(\frac{1}{\sqrt{N}} \sum_{\mathbf{k}} \hat{b}_{\mathbf{k}\sigma} e^{i\mathbf{k}'\cdot\vec{r}_j} \right) \right. \\ & \left. + \left(\frac{1}{\sqrt{N}} \sum_{\mathbf{k}} \hat{a}_{\mathbf{k}\sigma} e^{i\mathbf{k}\cdot\vec{r}_i} \right) \left(\frac{1}{\sqrt{N}} \sum_{\mathbf{k}} \hat{b}^{\dagger}_{\mathbf{k}\sigma} e^{-i\mathbf{k}'\cdot\vec{r}_j} \right) \right] \end{aligned}$$

Organizing the terms and substituting the position vectors of the jth atom $\vec{r}_j$ in terms of the relative vectors $\vec{r}_j = \vec{r}_i + \vec{\delta}_j$ we obtain:

$$\hat{H} = -\frac{t}{N} \sum_{<ij>,\sigma} \sum_{\mathbf{k}} \sum_{\mathbf{k}'} \left[\hat{a}^{\dagger}_{\mathbf{k}\sigma} e^{-i\mathbf{k}\cdot\vec{r}_i} \hat{b}_{\mathbf{k}\sigma} e^{i\mathbf{k}'\cdot\left(\vec{r}_i+\vec{\delta}_j\right)} \hat{a}_{\mathbf{k}\sigma} e^{i\mathbf{k}\cdot\vec{r}_i} \hat{b}^{\dagger}_{\mathbf{k}\sigma} e^{-i\mathbf{k}'\cdot\left(\vec{r}_i+\vec{\delta}_j\right)} \right]$$

Now, defining the function $g(\mathbf{k}')$ and its conjugate $g^{*}(\mathbf{k}')$ as

$$g(\mathbf{k}') = -t \sum_{l=1}^{3} e^{i\mathbf{k}'\cdot\vec{\delta}_l} \tag{2.7a}$$

$$g^{*}(\mathbf{k}') = -t \sum_{l=1}^{3} e^{-i\mathbf{k}'\cdot\vec{\delta}_l} \tag{2.7b}$$

and using the Kronecker Delta property in the reciprocal space:

$$\delta_{\mathbf{k},\mathbf{k}'} = \frac{1}{N} e^{\pm i(\mathbf{k}-\mathbf{k}')\cdot\vec{r}_i} \tag{2.8}$$

we have

$$\hat{H} = \sum_{\sigma}\sum_{\mathbf{k}}\sum_{\mathbf{k}'}\left[\hat{a}^{\dagger}_{\mathbf{k}\sigma}\hat{b}_{\mathbf{k}\sigma}\delta_{\mathbf{k},\mathbf{k}'}g(\mathbf{k}') + \hat{a}_{\mathbf{k}\sigma}\hat{b}^{\dagger}_{\mathbf{k}\sigma}\delta_{\mathbf{k},\mathbf{k}'}g^{*}(\mathbf{k}')\right]$$

Then:

$$\hat{H} = \sum_{\sigma}\sum_{\mathbf{k}}\sum_{\mathbf{k}'}\left[\hat{a}^{\dagger}_{\mathbf{k}\sigma}\hat{b}_{\mathbf{k}\sigma}g(\mathbf{k}) + \hat{a}_{\mathbf{k}\sigma}\hat{b}^{\dagger}_{\mathbf{k}\sigma}g^{*}(\mathbf{k})\right] \tag{2.9}$$

Defining a pseudo-spinor and its conjugate and a matrix 2 x 2 H_n

$$\psi_{\mathbf{k}\sigma} = \begin{bmatrix}\hat{a}_{\mathbf{k}\sigma}\\ \hat{b}_{\mathbf{k}\sigma}\end{bmatrix} \tag{2.10}$$

$$\psi^{*}_{\mathbf{k}\sigma} = \left[\hat{a}^{\dagger}_{\mathbf{k}\sigma}, \hat{b}^{\dagger}_{\mathbf{k}\sigma}\right] \tag{2.11}$$

$$H_N = \begin{bmatrix}0 & g(\mathbf{k})\\ g^{*}(\mathbf{k}) & 0\end{bmatrix} \tag{2.12}$$

we have

$$\psi^{*}_{\mathbf{k}\sigma}H_N\psi^{*}_{\mathbf{k}\sigma} = \hat{H} = \sum_{\sigma}\sum_{\mathbf{k}}\left[\hat{a}^{\dagger}_{\mathbf{k}\sigma}\hat{b}_{\mathbf{k}\sigma}g(\mathbf{k}) + \hat{a}_{\mathbf{k}\sigma}\hat{b}^{\dagger}_{\mathbf{k}\sigma}g^{*}(\mathbf{k})\right] \tag{2.13}$$

In matrix notation we can write,

$$\begin{bmatrix}0 & g(\mathbf{k})\\ g^{*}(\mathbf{k}) & 0\end{bmatrix}\begin{bmatrix}\hat{a}_{\mathbf{k}\sigma}\\ \hat{b}_{\mathbf{k}\sigma}\end{bmatrix} = E\begin{bmatrix}\hat{a}_{\mathbf{k}\sigma}\\ \hat{b}_{\mathbf{k}\sigma}\end{bmatrix}$$

to obtain the eigenvalues as

$$E = \pm|g(\mathbf{k})|. \tag{2.14}$$

As,

$$g(\mathbf{k}) = -t\sum_{l=1}^{3} e^{\left(i\mathbf{k}\cdot\vec{\delta}_l\right)} = -t\left[e^{\left(i\mathbf{k}\cdot\vec{\delta}_1\right)} + e^{\left(i\mathbf{k}\cdot\vec{\delta}_2\right)} + e^{\left(i\mathbf{k}\cdot\vec{\delta}_3\right)}\right]$$

and

$$g(\mathbf{k}) = -te^{i(ak_y)}\left[1 + e^{-i\frac{3ak_y}{2}}\left(\cos\frac{\sqrt{3}}{2}ak_x\right)\right] \tag{2.15}$$

We can write down the eigen-values are given by

$$E(\mathbf{k})_{\pm} = \pm t\left[3 + f(\mathbf{k})\right]^{\frac{1}{2}} \tag{2.16}$$

where

$$f(\mathbf{k}) = 2\cos(\sqrt{3}k_x a) + 4\cos\frac{3}{2}ak_y \cos\frac{\sqrt{3}}{2}ak_x \tag{2.17}$$

The equation (2.16) shows we have two symmetric solutions for the energy of the system. The positive energy E_+ and the negative energy E_-.

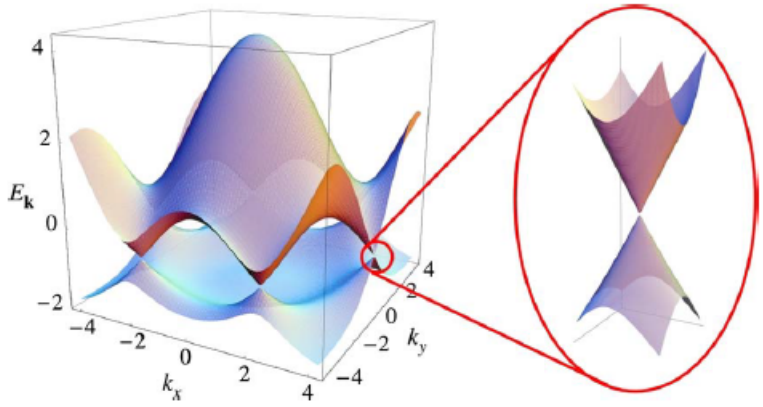

Figure 2.8: Graphene Energy Bands. Next to the Dirac points they form the Dirac cone. The energies E_+ and E_- are symmetrical around the Fermi Energy $E_F = 0$. The image is enlarged on the right, exhibiting the band energy close to the cone [5].

The figure (2.8) represents the energy bands in the first Brillouin zone described by the equations (2.16) and (2.17). The graphs show that the two energy bands (π and π^*) intersect at the so-called Dirac point where the energy is zero and the presence of the Dirac cones are observed due to the linear dispersion relation of graphene.

The chemical potential of the graphene can be considered in the tight-binding Hamiltonian as

$$H' = -\mu \sum_{<ij>,\sigma} \hat{n}_\sigma(R_i) \tag{2.18}$$

where $\hat{n}_\sigma(R_i)$ represents the number operator. Therefore eigen-energies are described by:

$$E(\mathbf{k})_\pm = \pm t\,[3 + f(\mathbf{k})]^{\frac{1}{2}} - \mu \tag{2.19}$$

Chapter 3

Theory of superconductivity.

3.1 Historical background.

The study of materials and the understanding of their physical properties have always attracted a lot of attention. The characterization of these materials is fundamental for its application. The conduction of these materials, whether thermal or electrical, is a physical quantity of great importance useful for their classification and understanding. In solid-state physics, the first attempt to simplify the modeling of metals was proposed by Drude. The above theory considered a crystalline lattice formed by oscillating ions (when the temperature is non-zero) surrounded by electrons known as free electrons. The ordered movement of these free electrons is responsible for creating an electric current. However, impurities or imperfections in the lattice that displace ions from their equilibrium positions generate the well-known electrical resistance[6] [30].

Metallic wires have electric resistance that opposes the current flow through the wire, thereby losing the electrical energy by turning it into thermal energy. Superconductors are materials with no electric resistance below a certain temperature: an electric current can flow through a superconductor without loosing any energy. A Fermi liquid is a theoretical model of interacting fermions that describes the normal state of most metals at low temperatures [31]. Electrons can move freely through a regular crystalline lattice, but any disruptions in the regularity of the lattice will obstruct their free flow and cause resistance, see Fig. (3.1). There are two main causes for electric resistance in wires. The imperfections in the crystalline lattice, such as those caused by impurity atoms or by vacancies. Each time an electron collides with an irregularity, it loses energy. Secondly, there are lattice vibrations. The vibrations are due to the phonons.

By early 1911 it was well known that the electric resistance in a metal decreased with temperature. Exactly what would happen approaching absolute zero was debated. Lord Kelvin believed that the flow of electrons in a material, which improved with decreasing temperature might actually stop altogether, the electrons becoming frozen in space. Thereby, the resistance

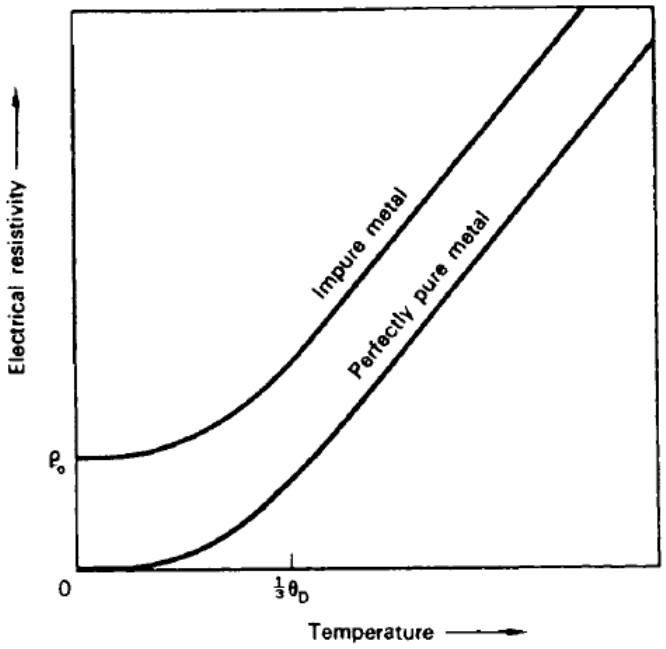

Figure 3.1: Graph representing resistance of pure and impure materials with temperature [6] .

at absolute zero could be infinitely high. Others including Onnes and Dewar argued that the decrease in resistance would continue in an regular manner, finally approaching a zero value at the zero temperature point. Finally in late 1911, Kamerlingh Onnes demonstrated that the resistance of mercury (Hg) decreased rapidly by a factor of at least 10^{10} at the onset of superconductivity, see Fig. (3.2). It continues to be superconducting below 4.15 K. He chose Hg as it could be easily purified. Soon it became very clear that the resistance of some other metals including mercury really does drop to zero below a certain temperature, known as critical temperature. Any current introduced into the loop would thereby continue to flow indefinitely [7].

Several groups continued the study in various parts of the world and years later the highest transition temperature or critical temperature among metals was observed for Niobium at T = 9.2k. However, more than half of the metals under the same experimental conditions, never become superconducting, such as gold, copper, bismuth and germanium.

Meissner and Ochsenfeld demonstrated that when a sphere of the above type is cooled below the transition temperature in a magnetic field it excludes the magnetic flux [32]. The same thing happens when the sphere is cooled first and then placed in a magnetic field. Hence superconductors are also perfect diamagnetic substances. A perfect conductor would resist a change of flux, while a superconductor expels any flux at all. Hence, a superconductor is not a theoretical perfect conductor as described by Maxwell's laws. A superconductor is a *perfect diamagnet*, a material which resists internal flux and it is the second hallmark of superconductors. This phenomena is known as the Meissner-Ochsenfeld effect, or more commonly referred to as the Meissner effect as illustrated in the figure below (3.3).

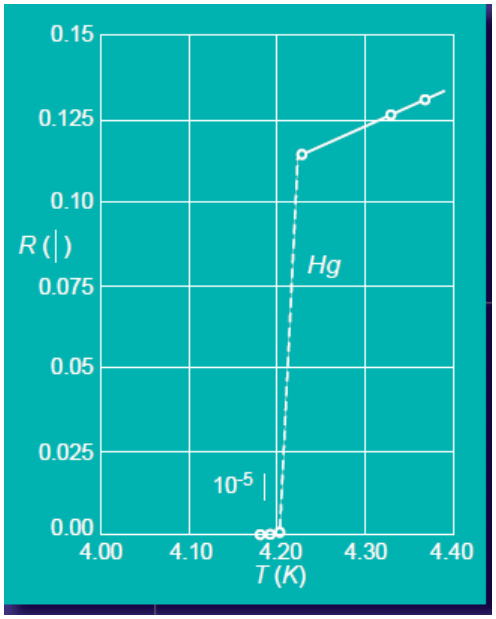

Figure 3.2: Graph of electrical resistance (in Ohm) by temperature (in Kelvin) for mercury (Hg). Highlighting the abrupt drop in electrical resistance at T = 4.2k obtained by Gilles Holst experimentally [7].

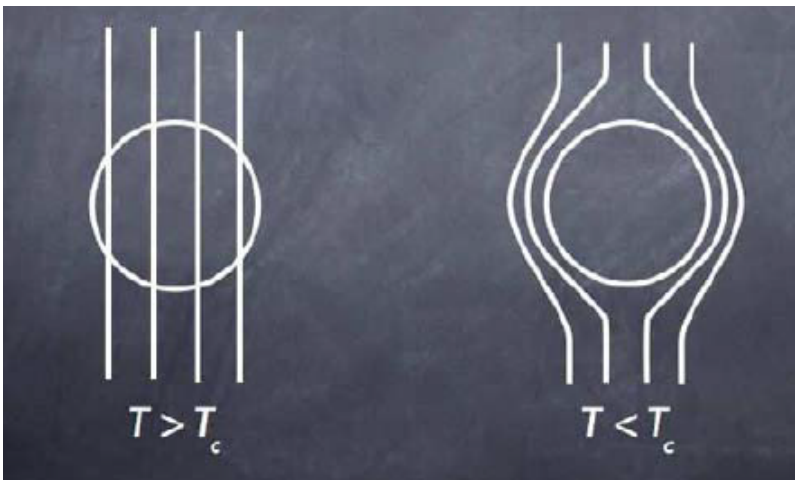

Figure 3.3: Illustration of the Meissner effect. In 1933 physicists Meissner and Ochsenfeld found that below critical temperatures the magnetic field is expelled from inside the material [8] .

In summary, a material is considered superconducting if it demonstrates zero resistivity and Meissner Effect below the critical temperature. The existence of such a reversible Meissner effect implies that superconductivity should be destroyed by a critical magnetic field, H_c, which is related thermodynamically to the free-energy difference between the normal and superconducting states in the zero field, the so-called condensation energy of the superconducting state. More precisely, *thermodynamic critical field,* H_c at temperature T is given by

$$H_c^2(T)/8\pi = f_N(T) - f_S(T) \tag{3.1}$$

where f_N and f_S are the Helmholtz free energies per unit volume in the respective phases at

zero field [10]. It was found empirically that $H_c(T)$ is quite well approximated by a parabolic law

$$H_c^2(T)/8\pi = H_c(0)[1-(T/T_c)^2] \tag{3.2}$$

Various other properties deserves to be mentioned. One of them is ξ_0, the coherence length at which electrons with energy close to Fermi energy are correlated. Moreover, they are responsible for supercurrents and provide a scale of the superconductivity wave functions . The other one is the penetration deep λ that measures how far the magnetic field penetrates the material surface, both are shown in the table below.

See in Fig. (3.4) a table that contains values of coherence length, critical temperature, penetration length and critical field of some conductors and compounds [7].

Superconductor	T_c *(K)*	$\lambda(0)$ *(Å)*	$\xi(0)$ *(Å)*	$H_{c2}(T)$
Nb	9.2	450	380	0.2
NbTi	9.5	1600	50	14
NbN	16	2000	50	16
Nb_3Sn	18.4	800	35	24
Nb_3Ge	23	-	35	38
$Ba_{0.6}K_{0.4}BiO_3$	31	2200	35	32
MgB_2	39	850	37	39
UPt_3	0.5	7800	200	2.8
UBe_{13}	0.9	3600	170	8
URu_2Si_2	1.2	-	130	8
$CeIrIn_5$	0.4	5300	250	1.0

Figure 3.4: Table of coherence length, Critical temperature, penetration length and critical field of some conductors and compounds [7].

The transition temperature also decreases with the increase in the average isotopic mass, called the isotope effect. The experimental results within each series of isotopes may be fitted by a relation of the form

$$M^{\alpha}T_c = \text{constant} \tag{3.3}$$

where M is the isotopic mass, T_c the critical temperature and α is a constant.

The α exponent has an approximate value of 0.45 to 0.50. Although there are exceptions regarding the veracity of the Isotope Effect for this term that approaches zero for Rubidium and Molybdenum, for example.

3.2 Transmission systems; Cold technology

Various uses have been suggested and observed for superconducting materials. Perhaps, the most trivial one is the transportation of electrical power from one place to another. Electricity is usually generated in large power stations, and transmitted along power lines to consumers who could be thousands of kilometers away. Typically, resistive heating in the metal wires of the transmission lines, usually made of cooper and aluminum, consumes 5 percent of the electrical power [33]. Hence, possible superconducting wires that could be able to reduce these losses would be a valuable investment for electricity suppliers

Superconductors do have various other practical uses, especially for specialized applications where cost is less significant. Among these are superconducting magnets. Wire made from a superconducting material is wound to form a solenoid and when high currents made to flow around these solenoids, it can produce strong magnetic fields with flux densities up to 20 Tesla's, roughly half a million times the strength of the earth's magnetic field [34]. The high current required for such enormous fields would cause conventional electromagnets to overheat.

Superconducting magnets are useful in magnetic resonance body scanners showing up details of the inside of a patient's body without the need for surgery or harmful radiation such as X-rays or gamma rays. Superconducting solenoids are also functional to levitate some of the world's fastest trains, known as "Maglev" trains.

Particle accelerators around the world also employ superconducting magnets. For example, superconducting magnets keep protons orbiting in a circular tunnel of more than 2 kilometers in diameter in laboratories around the world. The more energetic the particles being studied, the faster they move and stronger the field needed to keep them in the curved path. Only superconducting magnets are strong enough.

On a smaller-scale superconductors are used in electronic devices. A Josephson junction can function as an electronic switch which can switch very fast-within a picosecond (10^{-12} second). Such switches could substitute transistors to build supercomputers. The Josephson junctions are also worthwhile in electronic applications like the superconducting quantum interference device or SQUID. One or more junctions are formed into a loop, and when a magnetic field passes through the loop it includes a current. A SQUID can be used as an extremely sensitive device for measuring magnetic fields [35]. It is able to detect changes that are less than a billionth of the strength of the Earth's magnetic field. It is essential for various application like geologists use SQUIDs in search for minerals, chemists use them for monitoring corrosion and biophysicists use them for imaging activity in the human brain and heart, by detecting the magnetic fields arising from electric currents flowing in the body.

3.3 BCS Theory and Pairing Theory.

After the discovery of Onnes in 1911, many more superconducting materials were discovered in the laboratory in quick succession. Inspite of the few macroscopic theories that were put forward by F. and H. London [36], Ginzburg and Landau [37], but no suitable microscopic theory could explain this strange physical phenomenon. The microscopic theory that finally explained superconductivity was only developed after forty-six years of Onnes's discovery. In 1957, University of Illinois physicists John Bardeen, Leon Cooper and Robert Schrieffer put forth their microscopic theory which later became known by their initials as the BCS theory [38] . Bardeen, Cooper and Schrieffer received the Noble Prize in Physics in 1972 for their theory that revolutionized the quality of our understanding of superconductivity.

3.3.1 Cooper pairs and the origin of the attractive interaction.

Cooper pairs form the basis of the BCS theory [38]. In 1956, Cooper demonstrated that even a very weak attraction could bind pairs of electrons where two electrons over the full Fermi sea spontaneously form a bound Cooper pair if the regions ionic interaction is greater than the electron-electron repulsion [39]. Flux quantization and other experimental evidences support the formation of Cooper pairs and their role in the BCS theory. Hence this result is a consequence of the Fermi statistics and of the existence of the Fermi sea background.

In order to understand in detail, let us consider a simple model of two electrons added to a Fermi sea at T=0 with the condition that the extra electrons interact with each other but not with those in the sea, except via exclusion principle. Applying the general argument of Bloch, we expect the lowest energy state to have zero total momentum [10], so that the two electrons have equal and opposite momenta , see Figs. representations (3.5) .

An orbital wave function is given by

$$\psi_0(\mathbf{r_1}, \mathbf{r_2}) = \sum_{\mathbf{k}} g_{\mathbf{k}} e^{i\mathbf{k}.\mathbf{r_1}}\, e^{-i\mathbf{k}.\mathbf{r_2}} \tag{3.4}$$

where g_k is the weighting co-efficient, k is the momentum and r_1 and r_2 are the radial vectors. Taking into account the antisymmetry of the total wavefunction with respect to the exchange of the two electrons, ψ_0 is converted either to a sum of products of $\cos \mathbf{k}.(\mathbf{r}_1 - \mathbf{r}_2)$ with the antisymmetric singlet spin function $(\alpha_1\beta_2 - \beta_1\alpha_2)$ or to a sum of products of $\sin \mathbf{k}.(\mathbf{r}_1 - \mathbf{r}_2)$ with one of the symmetric triplet spin functions ($\alpha_1\alpha_2$, $\alpha_1\beta_2 + \alpha_2\beta_1$, $\beta_1\beta_2$). In these expressions α_1 refers to the spin up state of particle 1 and β_1 refers to the down state. Due to the existence of an attractive interaction, we expect the singlet coupling to have lower energy because the cosinusoidal dependence of its orbital wavefunction on $(\mathbf{r}_1 - \mathbf{r}_2)$ gives a larger

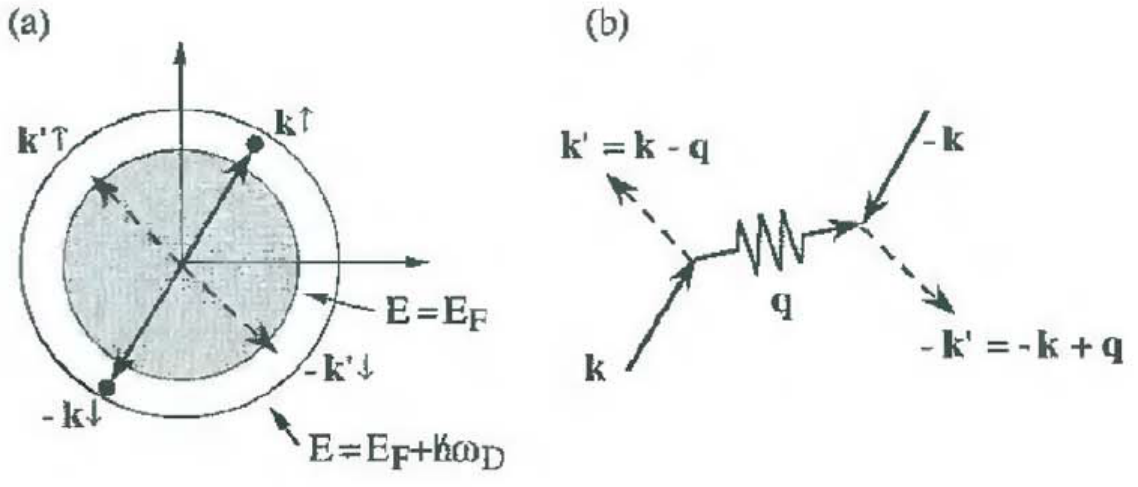

Figure 3.5: (a)Schematic representation of a single Cooper pair, added to the ground-state of a free-electron gas. Two "extras electrons" in the pair state $(\mathbf{k}\uparrow, -\mathbf{k}\downarrow)$ scatter freely to the pair states $(\mathbf{k}'\uparrow, -\mathbf{k}'\downarrow)$, in the energy region $E_F < E_{\mathbf{k}}, E'_{\mathbf{k}} < E_F + \hbar\omega_D$, where the phonon mediated attractive interaction is operative, and form a bond Cooper pair. (b) Schematic representation of a scattering of two electrons with wavevectors $(\mathbf{k}, -\mathbf{k})$ into $(\mathbf{k}', -\mathbf{k}')$ via the emission and subsequent absorption of a phonon of momentum $\hbar\mathbf{k}$ [9].

probability amplitude for the electrons to be near each other. Therefore,

$$\psi_0(\mathbf{r}_1 - \mathbf{r}_2) = \left[\sum_{k>k_F} g_k \cos \mathbf{k}.(\mathbf{r}_1 - \mathbf{r}_2)\right](\alpha_1\beta_2 - \beta_1\alpha_2) \tag{3.5}$$

where k_F is the Fermi momentum. Thereby, the Cooper pair equation can be written as

$$(\hat{E} - 2\epsilon_{\mathbf{k}})g_{\mathbf{k}} = \sum_{k'>k_F} V_{\mathbf{k}\mathbf{k}'} g'_{\mathbf{k}} \tag{3.6}$$

where $\hat{E}$ is the energy eigenvalue, $\epsilon_{\mathbf{k}}$ is the quasiparticle energy and $V_{\mathbf{k}\mathbf{k}'}$ is the interaction potential. Cooper binding is given by $B_c = 2E_F - \hat{E}$, where E_F is the Fermi energy. To understand the situation we can consider,

$$\begin{aligned} V_{\mathbf{k}\mathbf{k}'} &= -V, \quad \text{if } |\zeta_{\mathbf{k}}| < \hbar\omega_D \text{ and } |\zeta_{\mathbf{k}'}| < \hbar\omega_D; \\ &= 0, \quad \text{otherwise.} \end{aligned} \tag{3.7}$$

where $\hbar\omega_D$ is the Debye energy for photons in the lattice and $\zeta_{\mathbf{k}} = \epsilon_{\mathbf{k}} - E_F$, E_F being the Fermi energy. Thereby, we can write

$$\frac{1}{V} = \sum_{\mathbf{k}>k_F} (2\epsilon_{\mathbf{k}} - \hat{E})^{-1} \tag{3.8}$$

Hence, replacing the summation by an integration, with $N(0)$ denoting the density of states at the Fermi level for electrons of one spin orientation, we get:

$$\frac{1}{V} = N(0)\int_{E_F}^{E_F+\hbar\omega_D} \frac{d\epsilon}{2\epsilon - \hat{E}} = \frac{1}{2}N(0)\ln\frac{2E_F - \hat{E} + 2\hbar\omega_D}{2E_F - \hat{E}} \tag{3.9}$$

In most of the superconductors, it is found that $N(0)V < 0.3$. This allows the use of the so called *weak-coupling approximation*, valid for $N(0)V \ll 1$, in which the solution of the preceding equation can be written as:

$$\begin{aligned} E &\approx 2E_F - 2\hbar\omega_D\, e^{-2/N(0)V} \\ &\approx 2E_F - B_c \end{aligned} \tag{3.10}$$

Thus indeed, there is a bound state with negative energy with respect to the Fermi surface made up entirely of electrons with $k > k_F$, i.e., with kinetic energy in excess of E_F. The contribution to the energy of the attractive potential outweighs this excess kinetic energy, leading to binding regardless of how small V is.

3.3.2 BCS Equations

The Fermi sea is unstable against the formation of a bound Cooper pair when the net interaction is attractive. Hence, the pairs tend to condense until an equilibrium point is reached. The size of the Cooper pairs are much larger than the interparticle distance. This means that a large number of other pairs are present in between a given pair, as many as 10^6 other pairs. This large overlap of pairs contribute to a correlation of the other pairs. The collective state can be thought of as the Fermi gas being “condensed" into a “macromolecule" that includes the entire superconducting system. Therefore, the macromolecule remains superconducting until the gap energy is overcome.

At the transition temperature, the superconducting state becomes more favorable, and goes to a lower energy state. At temperatures higher than the transition temperature the Cooper pairs tend to dissociate leading to the normal state of the material. This explains the jump in the specific heat when the material moves from superconducting to normal state. Unlike liquid and gas phases, the phase transition from the normal state to the superconducting state is a second-order type. This means that when a material is cooled so that it becomes a superconductor, the transition takes place almost instantaneously without any latent heat, but nevertheless with a discontinuity in the specific heat. This can be seen from the abrupt drop in resistance within a small temperature range in the Fig. (3.2) .

In the microscopic theory, BCS (Bardeen, Cooper and Schrieffer) took a variational ansatz, designed to take maximum advantage of the Cooper condensation. In BCS theory the trial ground state $|\psi_g\rangle$ is taken to be,

$$|\psi_g\rangle = \prod_{\mathbf{k}}(u_{\mathbf{k}} + v_{\mathbf{k}}c^*_{\mathbf{k}\uparrow}c^*_{-\mathbf{k}\downarrow})|\phi_0\rangle \tag{3.11}$$

where $|\phi_0\rangle$ is the vacuum state with no particles present. The notation $c^*_{\mathbf{k}\uparrow}$ ($c_{\mathbf{k}\uparrow}$) denotes the creation (annihilation) operator of an electron with momentum $\mathbf{k}$ and spin up. $|u_{\mathbf{k}}|^2$ is the probability that the pair $(\mathbf{k}\uparrow, -\mathbf{k}\downarrow)$ is unoccupied and $|v_{\mathbf{k}}|^2$ is the probability that it is occupied. The complex variational amplitudes satisfy,

$$u_{\mathbf{k}} = u_{-\mathbf{k}} \tag{3.12}$$

$$v_{\mathbf{k}} = v_{-\mathbf{k}} \tag{3.13}$$

and the normalization requirement is

$$|u_{\mathbf{k}}|^2 + |v_{\mathbf{k}}|^2 = 1. \tag{3.14}$$

The product is over all $\mathbf{k}$ values allowed by box normalization conditions [40].

It should be noted that the variational state of equation (3.11) does not contain a fixed number of particles, since only the probabilities of pair occupation are specified. In the early days this was seen as a weakness of the formalism, although, for example, a superconducting specimen is normally probed by current leads, so that the number of electrons it contains is genuinely variable. That exists a "number- phase uncertainty relation", $\delta N \delta\phi \sim 1$ where δN is the uncertainty in the number of particles N and $\delta\phi$ is the uncertainty in the phase ϕ. It must be noted that there exists a phase difference by a factor of $e^{i\phi}$ between $u_{\mathbf{k}}$ and $v_{\mathbf{k}}$, where ϕ is independent of k and this is the phase for the BCS state. It can be shown that the variational energy is independent of the phase.

The "pairing Hamiltonian" or "reduced Hamiltonian" in terms of the creation and destruction operators is given by,

$$\mathcal{H} = \sum_{\mathbf{k}\sigma} \epsilon_{\mathbf{k}} n_{\mathbf{k}\sigma} + \sum_{\mathbf{kq}} V_{\mathbf{kq}} c^*_{\mathbf{k}\uparrow} c^*_{-\mathbf{k}\downarrow} c_{-\mathbf{q}\downarrow} c_{\mathbf{q}\uparrow} \tag{3.15}$$

where $c^*_{\mathbf{k}\sigma} c_{\mathbf{k}\sigma} = n_{\mathbf{k}\sigma}$ is the particle number operator, $V_{\mathbf{kq}}$ is the matrix element of the interaction potential. The solution can be obtained by using the variational approach as done in the original BCS paper [38].

As the number of particles is variable we need to minimize the expectation value $\langle\psi_g|\mathcal{H}|\psi_g\rangle$ subject to the constraint $\langle\psi_g|\hat{N}|\psi_g\rangle = N$. Here $\hat{N}$ is the number operator and N is the mean number of particles in the system. Hence by the method of undetermined multipliers we minimize the Hamiltonian

$$\delta\langle\psi_g \mid \mathcal{H} - \mu\hat{N} \mid \psi_g\rangle = 0$$

where μ is the chemical potential. The inclusion of $-\mu\hat{N}$ is mathematically equivalent to taking

zero of kinetic energy to be μ. Hence, writing more explicitly we get

$$\delta\langle\psi_g \mid \sum_{\mathbf{k}\sigma} \zeta_{\mathbf{k}} n_{\mathbf{k}\sigma} + \sum_{\mathbf{kq}} V_{\mathbf{kq}} c^*_{\mathbf{k}\uparrow} c^*_{-\mathbf{k}\downarrow} c_{-\mathbf{q}\downarrow} c_{\mathbf{q}\uparrow} \mid \psi_g\rangle = 0 \tag{3.16}$$

The number operator, $\hat{N}$ appears in conjunction with the kinetic energy operator, hence effectively the single particle energies $\zeta_{\mathbf{k}}$ are measured from E_F. Considering the ground state in equation (3.16) we get

$$\langle\psi_g \mid \mathcal{H} - \mu\hat{N} \mid \psi_g\rangle = \sum_{\mathbf{k}} 2\zeta_{\mathbf{k}} |v_{\mathbf{k}}|^2 + \sum_{\mathbf{kq}} V_{\mathbf{kq}} u_{\mathbf{k}} v_{\mathbf{k}} u_{\mathbf{q}} v_{\mathbf{q}} \tag{3.17}$$

which is to be minimized subject to the condition that $|u_{\mathbf{k}}|^2 + |v_{\mathbf{k}}|^2 = 1$. The condition for self consistency can be written as

$$\Delta_k = -\sum_{\mathbf{q}} \frac{\Delta_{\mathbf{q}}}{2E_{\mathbf{q}}} V_{\mathbf{kq}} = -\sum_{\mathbf{q}} \frac{\Delta_{\mathbf{q}}}{2(\Delta^2_{\mathbf{q}} + \zeta^2_{\mathbf{q}})^{1/2}} V_{\mathbf{kq}}, \tag{3.18}$$

Considering,

$$\begin{aligned} V_{\mathbf{kq}} &= -V, \quad \text{if } |\zeta_{\mathbf{k}}|, |\zeta_{\mathbf{q}}| < \hbar\omega_D; \\ &= 0, \quad \text{otherwise.} \end{aligned} \tag{3.19}$$

with V being a positive constant and Inserting this $V_{\mathbf{kq}}$ in (3.18), we find

$$\begin{aligned} \Delta_{\mathbf{k}} &= \Delta, \quad \text{if } |\zeta_{\mathbf{k}}| < \hbar\omega_D; \\ &= 0, \quad \text{otherwise.} \end{aligned} \tag{3.20}$$

Writing the summation in terms of an integral we can write,

$$\frac{1}{N(0)V} = \int_0^{\hbar\omega_D} \frac{d\zeta}{(\Delta^2_{\mathbf{q}} + \zeta^2_{\mathbf{q}})^{1/2}} = \sinh^{-1} \frac{\hbar\omega_D}{\Delta} \tag{3.21}$$

In the weak coupling limit we get,

$$\Delta = \frac{\hbar\omega_D}{\sinh[1/N(0)V]} \approx 2\hbar\omega_D e^{-1/N(0)V} \tag{3.22}$$

Physically, the parameter Δ is the minimum excitation energy, or the *energy gap*. A superconductor behaves as if there were a gap in energy of width 2Δ centered about the Fermi energy in the set of allowed one-electron levels.

BCS theory at nonzero temperature

The BCS state at $T = 0$ is described by the wave function ψ_g of equation (3.23).

$$|\psi_g\rangle = \prod_{\mathbf{k}} |\psi_{\mathbf{k}}\rangle \tag{3.23}$$

with

$$|\psi_{\mathbf{k}}\rangle = \prod_{\mathbf{k}} (u_{\mathbf{k}}|00\rangle + v_{\mathbf{k}}|11\rangle) \tag{3.24}$$

where $|00\rangle$ and $|11\rangle$ represents the unoccupied and the occupied pair respectively. At $T = 0$ only the pair states $|00\rangle$ and $|11\rangle$ occur, but for $T \geq 0$ it is required to consider the broken pair states $|01\rangle$ and $|10\rangle$. Specifically, $f_{\mathbf{k}}$ (Fermi function) is the probability that $|01\rangle$ and $|10\rangle$ are occupied, so that $(1 - 2f_{\mathbf{k}})$ is the probability that the pair state $\psi_{\mathbf{k}}$ of equation (3.24) is occupied. Hence we can redefine Δ for any value of temperature from the equation (3.18) as,

$$\begin{aligned} \Delta_{\mathbf{k}} &= -\sum_{\mathbf{q}} V_{\mathbf{kq}} u_{\mathbf{q}} v_{\mathbf{q}} (1 - 2f_{\mathbf{q}}) \\ &= -\sum_{\mathbf{q}} V_{\mathbf{kq}} \frac{\Delta_{\mathbf{q}}}{2E_{\mathbf{q}}} (1 - 2f_{\mathbf{q}}) \end{aligned} \tag{3.25}$$

As $E_{\mathbf{k}}$ is an excitation energy, shows that, just at zero temperature, $|\Delta_{\mathbf{k}}|$ is the energy gap and $E_{\mathbf{k}}$ must be a positive quantity $\geq |\Delta_{\mathbf{k}}|$. Since $f_{\mathbf{q}}$ is the thermal occupation probability, this shows that $\Delta_{\mathbf{q}}$ is temperature dependent. The usual Fermi function is defined as

$$f_{\mathbf{q}} = (e^{\beta E_{\mathbf{q}}} + 1)^{-1} \tag{3.26}$$

where $\beta = 1/k_B T$. Since $E_{\mathbf{q}} \geq \Delta$, $f_{\mathbf{q}} \to 0$ at $T = 0$ for all $\mathbf{q}$.

Hence considering equations (3.25) (3.26) we get,

$$\Delta_{\mathbf{k}} = -\sum_{\mathbf{q}} V_{\mathbf{kq}} \frac{\Delta_{\mathbf{q}}}{2E_{\mathbf{q}}} \tanh \frac{E_{\mathbf{q}}}{2k_B T}. \tag{3.27}$$

Making use of the BCS approximation that $V_{\mathbf{kq}} = -V$ and $\Delta_{\mathbf{k}} = \Delta_{\mathbf{q}} = \Delta$, the self consistency condition becomes,

$$\frac{1}{V} = \frac{1}{2} \sum_{\mathbf{k}} \frac{\tanh(\beta E_{\mathbf{k}}/2)}{2E_{\mathbf{k}}}; \tag{3.28}$$

a temperature dependent form of the gap equation. See the representations f Δ Figs. (3.6) (3.7).

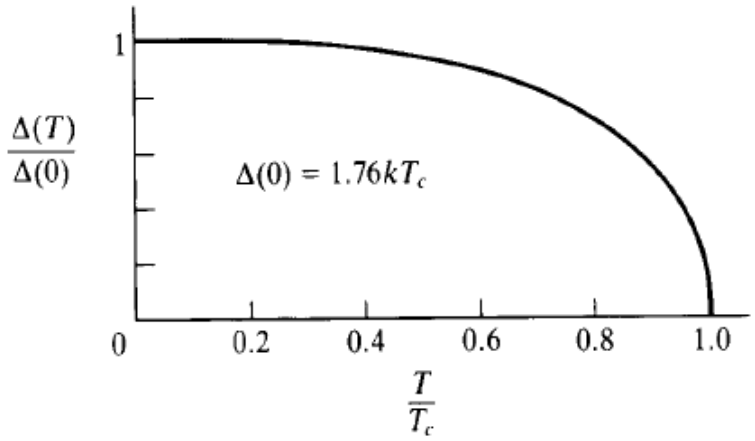

Figure 3.6: $\Delta(T)/\Delta_0$ vs T/T_C where Δ_0 is the zero temperature order parameter. The normal state persists for $T > T_C$ [10].

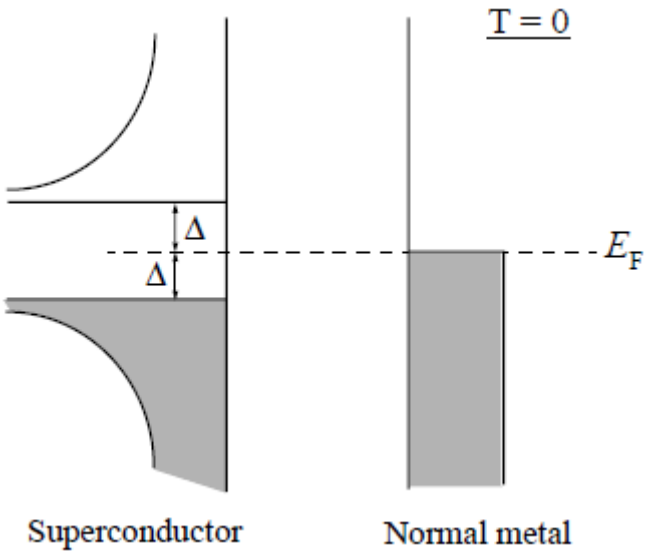

Figure 3.7: Representation of the gap around the Fermi energy comparing the superconducting state and the normal state(T=0) [7].

3.4 Thermodynamic parameter - Specific heat

The temperature dependencies of the order parameter can be determined from equation (3.27). Thereby, the electronic entropy is given by

$$S_S(T) = -2k_B \sum_{\mathbf{k}} [(1 - f_{\mathbf{k}}) \ln(1 - f_{\mathbf{k}}) + f_{\mathbf{k}} \ln f_{\mathbf{k}}]. \tag{3.29}$$

Given $S_S(T)$, the specific heat can be calculated by using

$$C_S(T) = T\frac{dS_S}{dT} = -\beta\frac{dS_S}{d\beta}.$$

Hence using equation (3.29) we can write

$$C_S(T) = 2\beta k_B \sum_{\mathbf{k}} -\frac{\partial f_{\mathbf{k}}}{\partial E_{\mathbf{k}}}\left(E_{\mathbf{k}}^2 - \frac{1}{2}\beta\frac{d\Delta_{\mathbf{k}}^2}{d\beta}\right) \tag{3.30}$$

The first term in the above equation is the usual one coming from the redistribution of quasi particles among the various energy states as temperature changes. The second term describes the effect of the temperature-dependent gap. The normal specific heat $C_N(T)$ can be obtained from the above expression by putting $\Delta(T) = 0$. Replacing $E_{\mathbf{k}}$ by $|\zeta_{\mathbf{k}}|$ in (3.30) one gets

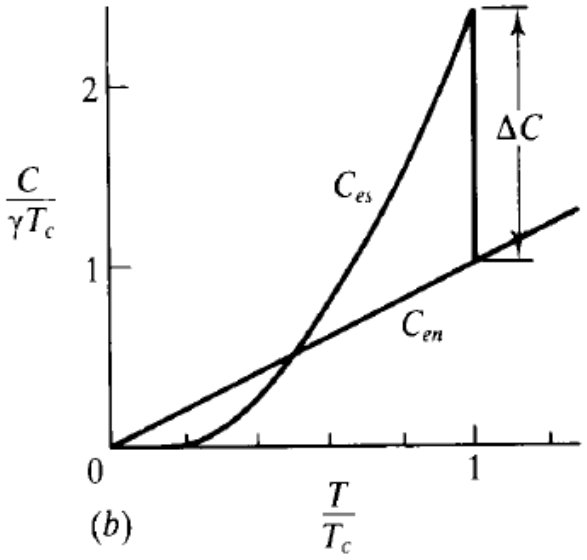

Figure 3.8: Graph of specific heat normalized with respect to temperature. C_S is continuous at the critical temperature so there is a second order transition [10].

$$C_N(T) = \gamma T = \frac{2\pi^2}{3}N(0)k_B^2 T \tag{3.31}$$

which is continuous at T_c. There is a discontinuity in the superconducting specific heat C_S at $T = T_c$ due to the fact that the second term of equation (3.30) is finite below T_c where $d\Delta^2/dT$ is large, but is zero above T_c. This jump indicates that the normal superconducting transition is a second-order phase transition. The jump in the specific heat $\Delta C = (C_S - C_N)|_{T_c}$ can be found to be.

$$\Delta C = \sum_q \frac{d\Delta_q^2}{dT}\frac{\partial f}{\partial E_q} \tag{3.32}$$

See its representations in Fig. (3.8).

Chapter 4

Superconducting states of single-layer graphene.

Superconductivity in graphene has attracted a lot of attention in recent years. Several studies on the transport mechanism in graphene demonstrates the observation of the proximity induced superconductivity in graphene [41]. The energy spectrum with linear dispersion in the reciprocal and peculiar space and the Dirac nature of the quasiparticles allows the presence of supercurrents in long junctions [42] [43]. Several theoretical studies has been performed on the differential conductance in normal-superconductor interfaces [44] . Josephson current in graphene SNS junction was considered in [45] [46]. The importance of the above studies lie in the various possible applications like current switches [47], spin-current filter [48], and many more.

The above advancement in the tunneling processes stimulated a lot of enthusiasm in making graphene an intrinsic superconductor. Various parent compounds like CaC_6 and KC_8 are low-temperature superconductors although graphite is non-superconducting [49] [50]. However, several possibilities of observing superconductivity have been proposed till date like the plasmon-mediate mechanism [13], proximity effect on adsorption of metallic atoms electronic mechanism involving Van Hove singularity [51], presence of spin-density wave or a charge-density wave and other competitive phases [52] [53].

Moreover, possible superconductivity in graphene was demonstrated through different calculations that demonstrate that for pure graphene the electron–phonon coupling constant is very weak and phonon-mediated superconductivity does not occur [54]. Nevertheless, recently first-principles calculations predicted the presence of superconductivity in chemically doped graphene. For example, superconductivity with critical temperatures around 8k and 17k was detected in lithium-doped graphene (LiC_6 and Li_2C_6 , respectively) [55]. T_c around 13k and 30k were demonstrated for electron-doped and hole-doped graphene, respectively [56] [57]. Furthermore, hole-doped graphene was predicted to be a high T_c superconductor with a transition temperature above 80k [58]. Hence doping graphene seems to be a fruitful way of producing superconductivity in graphene.

Regardless of the microscopic origin, the superconducting state in graphene can be studied considering the symmetries and the possible pairing observed in graphene. The article "Superconducting States of Pure and Doped Graphene" by Bruno Uchoa and A.H. Castro Neto [13] serves as an exponent of research in this area, including for this dissertation, serving as a basis for a concise understanding of the addressed subject. It explains how the study of the superconducting state in pure and doped graphene is carried out, with an emphasis on retarded Green equation methods, plasmon quantizations and based on proximity effects to induce cooper pairs in pure graphene making it an intrinsic superconductor [11] [5] [13].The presence of superconductivity demonstrates that Cooper pairs can propagate coherently in graphene. Graphene is a zero-gap semiconductor, but bilayer graphene has been shown to be a tunable gap semiconductor. Hence, modifying graphene it might be possible not only to obtain the gap but also create a superconductor.

In ref. [11] they exhibit a mean-field phase diagram for spin-singlet superconductivity where two types of pairing are observed. One is the s wave pairing and another of $p+ip$ orbital symmetry. The s wave demonstrates an isotropic dependence on momentum k whereas the $p+ip$ dependence can be seen from the figure below (4.1). From the orbital point of view of the crystalline lattice, its composition only by carbon atoms in bonds of the type sp^2, mixed bonds of the atomic orbitals of the band s and band p form the honeycomb structure. The resulting hybridization comprises low density sub-levels that even at the lowest temperature close to absolute zero does not generate the need for an intraband model study related to this phenomenon. The maximum p wave infers in the matching symmetry around the Dirac points. Such symmetry is lost as we move away from the points.

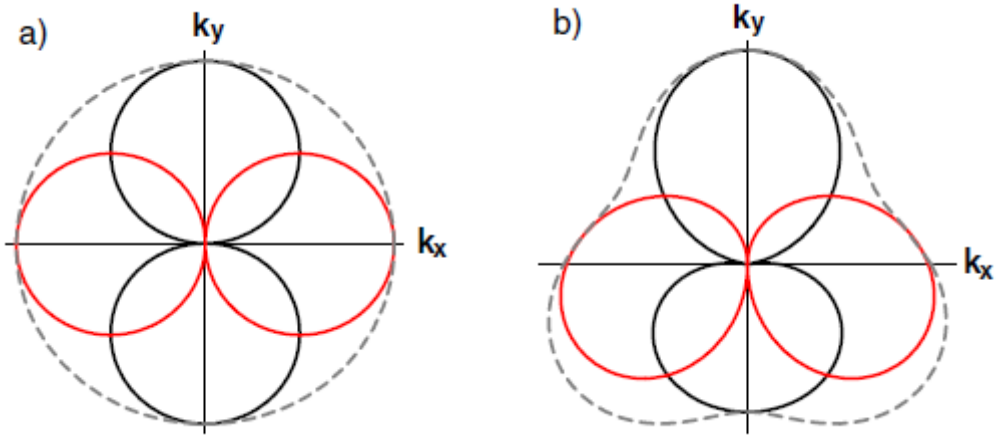

Figure 4.1: a)Symmetry of the p wave in the space of moment near the points of Dirac.b) The symmetry is broken away from the points of Dirac. The gray lines represent the real space and the black the imaginary space [11].

The mean-field phase diagram demonstrates that both the above types can be observed but with an substantial dependence on the chemical potential and the relative values of the

interaction parameters. Other types of symmetry have also been proposed that could explain the presence of superconductivity in graphene. Black Schaeffer and Doniach [45] described a pairing of the type $\Delta_{1,j} = \Delta_1 e^{i(2\pi/3)j}$ with $j = 1, 2, 3$ for the three neighbors of the site leading to in $d_{x^2-y^2}$ symmetry in real space and d_{xy} in imaginary space . Despite the effort, this pairing does not preserve all the translation and rotation symmetries of the lattice.

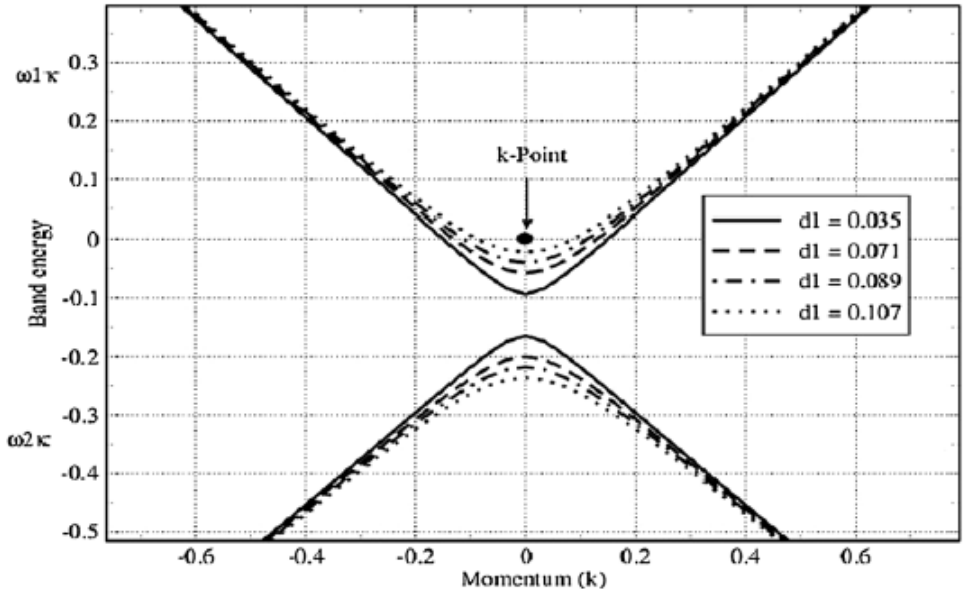

Figure 4.2: Energy band with respect to moment k for different substrates. For different values of state density $d1 = 0.0035, 0.0071, 0.0089, 0.107$ in order to open a gap in the original energy band of graphene [12].

When graphene is placed on substrates to induce cooper pairs in the sample, gaps of a small order of magnitude were observed (approximately 100 meV) and 250meV for silicone substrates [12]. On the other hand,in the honeycomb structure with Boron Nitride (BN) atoms, excitation energies with a gap band of 5.56eV has been observed [12]. On different semiconductor surfaces such as silicon, lead, and tin, interaction energies of the order of $g_0 = 3.3t = 9.34$ eV and $g_1 = 2.0t = 5.6$eV are observed. Figure (4.2) shows the momentum dependencies of the superconducting gaps for various values of the density of the surface.

In the next section the Model Hamiltonian is considered in our study to demonstrate the presence of superconductivity in graphene using a mean-field approximation. The temperature dependencies of the order parameter and also the dependencies on the interaction parameters will be considered.

4.1 Model Hamiltonian

The Hamiltonian considered to study superconductivity in Graphene can be given by:

$$H = H_t + H_p \tag{4.1}$$

where the term H_t is the tight-binding Hamiltonian for graphene considering the hopping parameter and the chemical potential. H_t can be written as

$$H_t = -t \sum_{<ij>,\sigma=\pm} (a^\dagger_{i\sigma} b_{j\sigma} + h.c.) - \mu \sum_{i,\sigma=\pm} (a^\dagger_{i\sigma} a_{i\sigma} + b^\dagger_{i\sigma} b_{i\sigma}) \tag{4.2}$$

The second term H_p represents the electron-electron interaction and is given by:

$$H_P = \frac{g_0}{2} \sum_{i,\sigma} [a^\dagger_{i\sigma} a_{i\sigma} a^\dagger_{i-\sigma} a_{i-\sigma} + b^\dagger_{i\sigma} b_{i\sigma} b^\dagger_{i-\sigma} b_{i-\sigma}] + g_1 \sum_{<ij>} \sum_{\sigma,\sigma'} a^\dagger_{i\sigma} a_{i\sigma} b^\dagger_{j\sigma'} b_{j\sigma'} \tag{4.3}$$

t - is the hopping parameter, μ - Represents the chemical potential, g_0 and g_1 are on-site and the nearest-neighbor electron-electron interaction energies, respectively. The operators $a^\dagger_{i\sigma}, \hat{a}_{i\sigma}$ are the creation and destruction operates in sublattice A which create or destroy the electron at points in the vicinity of its i spin ρ sublattice. The operators $\hat{b}^\dagger_{i\sigma}, b_{i\sigma}$ perform the same process of creation and destruction in sublattice B. $i(j)$ labels the sites in sublattice $A(B)$ and σ is the spin. H_P represents the electron-electron interaction of opposite spins. g_0 and g_1 are the on-site and nearest neighbor elctron electron interaction energies.

If $\mu = 0$ we have particle-hole symmetry around the Dirac points, otherwise this symmetry is broken the term that surrounds it in the Hamiltonian introduces an electron surface ($\mu < 0$) or holes ($\mu > 0$) around the Dirac points producing a finite density of states.

The order parameters for the singlet spin are:

for s wave:

$$\Delta_0 = < a_{i\downarrow} a_{i\uparrow} > = < b_{i\downarrow} b_{i\uparrow} >$$

and for the $p + ip$ wave :

$$\Delta_{1ij} = < a_{i\downarrow} b_{j\uparrow} - b_{i\uparrow} a_{j\downarrow} >$$

where we defining both as a real number. Then $\Delta^*_0 = \Delta_0$ and $\Delta^*_1 = \Delta_1$.

Using the mean field theory (see appendix C.5) the electron-electron interaction of the same site of sublattice A, can be written as

$$\begin{aligned} \sum_{i,\sigma} g_0 a^\dagger_{i\sigma} a_{i\sigma} a^\dagger_{i-\sigma} a_{i-\sigma} &= \sum_{i,\sigma} [g_0 < a^\dagger_{i\sigma} a^\dagger_{i-\sigma} > a_{i\sigma} a_{i-\sigma} + g_0 < a_{i\sigma} a_{i-\sigma} > a^\dagger_{i\sigma} a^\dagger_{i-\sigma} \\ &- g_0 < a^\dagger_{i\sigma} a^\dagger_{i-\sigma} >< a_{i\sigma} a_{i-\sigma} >]. \end{aligned}$$

Hence,

$$\sum_{i,\sigma} g_0 a^\dagger_{i\sigma} a_{i\sigma} a^\dagger_{i-\sigma} a_{i-\sigma} = \sum_{i,\sigma} [g_0 \Delta^*_0 a_{i\sigma} a_{i-\sigma} + g_0 \Delta_0 a^\dagger_{i\sigma} a^\dagger_{i-\sigma} - g_0 \Delta^2_0] \tag{4.4}$$

Similary for the sublattice B we have

$$\begin{aligned}\sum_{i,\sigma} g_0 b^\dagger_{i\sigma} b_{i\sigma} b^\dagger_{i-\sigma} b_{i-\sigma} &= \sum_{i,\sigma} [g_0 < b^\dagger_{i\sigma} b^\dagger_{i-\sigma} > b_{i\sigma} b_{i-\sigma} + g_0 < b_{i\sigma} b_{i-\sigma} > b^\dagger_{i\sigma} b^\dagger_{i-\sigma} \\ &- g_0 < b^\dagger_{i\sigma} b^\dagger_{i-\sigma} >< b_{i\sigma} b_{i-\sigma} >]\end{aligned}$$

giving rise to

$$\sum_{i,\sigma} g_0 b^\dagger_{i\sigma} b_{i\sigma} b^\dagger_{i-\sigma} b_{i-\sigma} = \sum_{i,\sigma} [g_0 \Delta^*_0 b_{i\sigma} b_{i-\sigma} + g_0 \Delta_0 b^\dagger_{i\sigma} b^\dagger_{i-\sigma} - g_0 \Delta^2_0]$$

Now for the electron-electron interaction of the nearest neighbors we can write

$$g_1 \sum_{<ij>} \sum_{\sigma,\sigma'} a^\dagger_{i\sigma} a_{i\sigma} b^\dagger_{j\sigma'} b_{j\sigma'} = g_1 \sum_{<ij>} [a^\dagger_{i\uparrow} a_{i\uparrow} b^\dagger_{j\downarrow} b_{j\downarrow} + a^\dagger_{i\downarrow} a_{i\downarrow} b^\dagger_{j\uparrow} b_{j\uparrow}] \tag{4.5}$$

Hence, the above term can be rewritten as:

$$g_1 \sum_{<ij>} \sum_{\sigma,\sigma'} a^\dagger_{i\sigma} a_{i\sigma} b^\dagger_{j\sigma} b_{j\sigma} = g_1 \sum_{<ij>} (-B^\dagger_{ij} B_{ij} + D^\dagger_{ij} D_{ij}) \tag{4.6}$$

where $D_{ij} = a_{i\uparrow} b_{j\downarrow} - a_{i\downarrow} b_{j\uparrow}$ e $B_{ij} = a^\dagger_{i\uparrow} b_{j\uparrow} + a^\dagger_{i\downarrow} b_{j\downarrow}$.

The above relation can be demonstrated remembering the anti-commutation relationships of the fermion operators of the two sublattices of graphene. (see appendix A.7). For sub lattice A, we have

$$\sum_{\sigma,\sigma'} [a_\sigma, a^\dagger_{\sigma'}] = \sum_{\sigma,\sigma'} \delta_{\sigma,\sigma'} \tag{4.7}$$

Similar relations for the B sublattice can also be written. Considering the expression $B_{ij} = a^\dagger_{i\uparrow} b_{j\uparrow} + a^\dagger_{i\downarrow} b_{j\downarrow}$ we can write down the product of the operators as

$$\begin{aligned}-B^\dagger_{ij} B_{ij} &= (b^\dagger_{j\uparrow} a_{i\uparrow} + b^\dagger_{j\downarrow} a_{i\downarrow})(a^\dagger_{i\uparrow} b_{j\uparrow} + a^\dagger_{i\downarrow} b_{j\downarrow}) \\ &= -b^\dagger_{j\uparrow} a_{i\uparrow} a^\dagger_{i\uparrow} b_{j\uparrow} - b^\dagger_{j\downarrow} a_{i\downarrow} a^\dagger_{i\uparrow} b_{j\uparrow} \\ &\quad -b^\dagger_{j\uparrow} a_{i\uparrow} a^\dagger_{i\downarrow} b_{j\downarrow} - b^\dagger_{j\downarrow} a_{i\downarrow} a^\dagger_{i\downarrow} b_{j\downarrow}\end{aligned}$$

In the same manner for the operator D_{ij}, we get

$$\begin{aligned} D_{ij}^{\dagger}D_{ij} &= (b_{j\downarrow}^{\dagger}a_{i\uparrow}^{\dagger} - b_{j\uparrow}^{\dagger}a_{i\downarrow}^{\dagger})(a_{i\uparrow}b_{j\downarrow} - a_{i\downarrow}b_{j\uparrow}) \\ &= b_{j\downarrow}^{\dagger}a_{i\uparrow}^{\dagger}a_{i\uparrow}b_{j\downarrow} - b_{j\downarrow}^{\dagger}a_{i\downarrow}^{\dagger}a_{i\uparrow}b_{j\downarrow} \\ &-b_{j\downarrow}^{\dagger}a_{i\uparrow}^{\dagger}a_{i\downarrow}b_{j\uparrow} + b_{j\uparrow}^{\dagger}a_{i\downarrow}^{\dagger}a_{i\downarrow}b_{j\uparrow} \end{aligned}$$

Hence, applying the anti-commutation relations and thereby adding the terms we have,

$$\begin{aligned} g_1 \sum_{<ij>}[-B_{ij}^{\dagger}B_{ij} + D_{ij}^{\dagger}D_{ij}] &= g_1 \sum_{<ij>}[a_{i\uparrow}^{\dagger}a_{i\uparrow}b_{j\downarrow}^{\dagger}b_{j\downarrow} + a_{i\downarrow}^{\dagger}a_{i\downarrow}b_{j\uparrow}^{\dagger}b_{j\uparrow}] \\ &+ g_1 \sum_{<ij>}[a_{i\uparrow}^{\dagger}a_{i\uparrow}b_{j\uparrow}^{\dagger}b_{j\uparrow} + a_{i\downarrow}^{\dagger}a_{i\downarrow}b_{j\downarrow}^{\dagger}b_{j\downarrow}] \end{aligned} \tag{4.8}$$

Mean-field theory has the enormous advantage of being mathematically simple, and it is almost invariably the first approach taken to predict phase diagrams and properties of new experimental systems. Therefore,

$$\begin{aligned} g_1 \sum_{<ij>}\sum_{\sigma,\sigma'} a_{i\sigma}^{\dagger}a_{i\sigma}b_{j\sigma'}^{\dagger}b_{j\sigma'} &= g_1 \sum_{<ij>}[< D_{ij} > D_{ij}^{\dagger} + < D_{ij}^{\dagger} > D_{ij} - < D_{ij}^{\dagger} >< D_{ij} >] \\ &+ g_1 \sum_{<ij>}[< B_{ij} > B_{ij}^{\dagger} + < B_{ij}^{\dagger} > B_{ij} - < B_{ij}^{\dagger} >< B_{ij} >] \end{aligned} \tag{4.9}$$

As we already know that $< B_{ij} >= 0$, we have:

$$g_1 \sum_{<ij>}\sum_{\sigma,\sigma'} a_{i\sigma}^{\dagger}a_{i\sigma}b_{j\sigma'}^{\dagger}b_{j\sigma'} = g_1 \sum_{<ij>}[< D_{ij} > D_{ij}^{\dagger} + < D_{ij}^{\dagger} > D_{ij} - < D_{ij}^{\dagger} >< D_{ij} >]$$

$$\begin{aligned} g_1 \sum_{<ij>}\sum_{\sigma,\sigma'} a_{i\sigma}^{\dagger}a_{i\sigma}b_{j\sigma'}^{\dagger}b_{j\sigma'} &= g_1 \sum_{<ij>}[\Delta_{1ij}(a_{i\uparrow}^{\dagger}b_{j\downarrow}^{\dagger} - a_{i\downarrow}^{\dagger}b_{j\uparrow}^{\dagger}) + \Delta_{1ij}^{\dagger}(a_{i\uparrow}b_{j\downarrow} - a_{i\downarrow}b_{j\uparrow})] \\ &- 3g_1\Delta_1^2 \end{aligned} \tag{4.10}$$

where 3 represents the sum of the three closest neighbors. Considering all the above terms and then rewriting the Hamiltonian H_P, we have

$$\begin{aligned} H_P &= \sum_i g_0[\Delta_0^{*}a_{i\uparrow}a_{i\downarrow} + \Delta_0 a_{i\uparrow}^{\dagger}a_{i\downarrow}^{\dagger} + \Delta_0^{*}b_{i\uparrow}b_{i\downarrow} + \Delta_0 b_{i\uparrow}^{\dagger}b_{i\downarrow}^{\dagger}] \\ &+ \sum_{<ij>} g_1[\Delta_{1ij}(a_{i\uparrow}^{\dagger}b_{j\downarrow}^{\dagger} - a_{i\downarrow}^{\dagger}b_{j\uparrow}^{\dagger}) + \Delta_{1ij}^{\dagger}(a_{i\uparrow}b_{j\downarrow} - a_{i\downarrow}b_{j\uparrow})] \\ &-g_0\frac{\Delta_0^{*}\Delta_0}{2} - g_0\frac{\Delta_0^{*}\Delta_0}{2} - 3g_1\Delta_1^2 \end{aligned} \tag{4.11}$$

Defining $E_0 = -g_0\Delta_0^2 - 3g_1\Delta_1^2$, we have:

$$H_P = E_0 + g_0\Delta_0 \sum_i (a^\dagger_{i\uparrow}a^\dagger_{i\downarrow} + b^\dagger_{i\uparrow}b^\dagger_{i\downarrow}) + h.c + \sum_{<ij>} g_1\Delta_{1ij}(a^\dagger_{i\uparrow}b^\dagger_{j\downarrow} - a^\dagger_{i\downarrow}b^\dagger_{j\uparrow}) + h.c \quad (4.12)$$

In Nambu bases considering the wave function to be $\Psi_k = (a_{\mathbf{k}\uparrow}, b_{\mathbf{k}\uparrow}, a^\dagger_{-\mathbf{k}\downarrow}b^\dagger_{-\mathbf{k}\downarrow})$, we can rewrite the tight-binding Hamiltonian as:

$$H = \sum_{\mathbf{k}} \Psi^\dagger_{\mathbf{k}} H \Psi_{\mathbf{k}} + E_0 \quad (4.13)$$

But to write the matrix we first need to write the Fourier transform of the Hamiltonian in $\mathbf{k}$ space. So now considering the Fourier transform

$$a_\sigma(R_i) = \frac{1}{\sqrt{N}} \sum_{\mathbf{k}} \exp^{i\overline{\mathbf{k}}.\overline{R}_i} a_{\mathbf{k}\sigma} \quad (4.14)$$

and

$$b_\sigma(R_j) = \frac{1}{\sqrt{N}} \sum_{\mathbf{k}} \exp^{i\overline{\mathbf{k}'}.\overline{R}_j} b_{\mathbf{k}'\sigma} \quad (4.15)$$

and its conjugate transform:

$$a^\dagger_\sigma(R_i) = \frac{1}{\sqrt{N}} \sum_{\mathbf{k}} \exp^{-i\overline{\mathbf{k}}.\overline{R}_i} a^\dagger_{\mathbf{k}\sigma}$$

$$b^\dagger_\sigma(R_j) = \frac{1}{\sqrt{N}} \sum_{\mathbf{k}} \exp^{-i\overline{\mathbf{k}}.\overline{R}_j} b^\dagger_{\mathbf{k}\sigma}$$

where $\overline{\mathbf{k}}$ and $\overline{\mathbf{k}}'$ are the vectors of the first Brillouin zone in sublattices A and B , respectively. Now representing the operators in that space.

$$\begin{aligned} \sum_{<ij>,\sigma} a^\dagger_\sigma(R_i)b_\sigma(R_j) &= \sum_{j=1}^{3} \sum_{i\sigma} \frac{1}{N} \sum_{\mathbf{k},\mathbf{k}'} \exp^{-i\mathbf{k}'\delta_j} \exp^{-i(\mathbf{k}-\mathbf{k}').R_i} a^\dagger_{\mathbf{k}\sigma} b_{\mathbf{k}'\sigma} \\ &= \sum_{j=1}^{3} \sum_{\mathbf{k}\sigma} \exp^{i\mathbf{k}'\delta_j} a^\dagger_{\mathbf{k}\sigma} b_{\mathbf{k}'\sigma} \end{aligned} \quad (4.16)$$

where does the Dirac Delta function used for our calculation is given by $\delta_{\mathbf{k}\mathbf{k}'} = \frac{1}{N}\sum_i \exp^{-i(\mathbf{k}-\mathbf{k}').R_i}$.

Similarly,

$$\sum_{<ij>,\sigma} a^\dagger_\sigma(R_i)a_\sigma(R_j) = \frac{1}{N} \sum_{<ij>,\sigma} \sum_{\mathbf{k}\mathbf{k}'} \exp^{-i\overline{\mathbf{k}R_i}} \exp^{i\overline{\mathbf{k}'R_j}} a^\dagger_{\mathbf{k}\sigma} a_{\mathbf{k}'\sigma} \quad (4.17)$$

$$\sum_{i,\sigma} a^\dagger_{i\sigma} a_{i\sigma} = \sum_{\mathbf{k},\sigma} a^\dagger_{\mathbf{k}\sigma} a_{\mathbf{k}\sigma} \quad (4.18)$$

Similarly we have:

$$\sum_{<ij>,\sigma} b^{\dagger}_{\sigma}(R_i) b_{\sigma}(R_j) = \frac{1}{N} \sum_{<ij>,\sigma} \sum_{\mathbf{k}\mathbf{k}'} \exp^{-i\bar{\mathbf{k}}R_i} \exp^{i\bar{\mathbf{k}'}R_j} b^{\dagger}_{\mathbf{k}\sigma} b_{\mathbf{k}'\sigma} \tag{4.19}$$

$$\sum_{i,\sigma} b^{\dagger}_{i\sigma} b_{i\sigma} = \sum_{\mathbf{k},\sigma} b^{\dagger}_{\mathbf{k}\sigma} b_{\mathbf{k}\sigma} \tag{4.20}$$

Specifying the spins we can write the relevant terms as

$$\sum_{<ij>} a^{\dagger}_{i\uparrow} a^{\dagger}_{j\downarrow} = \sum_{\mathbf{k}} a^{\dagger}_{\mathbf{k}\uparrow} a^{\dagger}_{-\mathbf{k}\downarrow} \tag{4.21}$$

$$\sum_{<ij>} b^{\dagger}_{i\uparrow} b^{\dagger}_{j\downarrow} = \sum_{\mathbf{k}} b^{\dagger}_{\mathbf{k}\uparrow} b^{\dagger}_{-\mathbf{k}\downarrow} \tag{4.22}$$

Moreover, we get,

$$\begin{aligned} \sum_{<ij>} a^{\dagger}_{i\uparrow} b^{\dagger}_{j\downarrow} &= \sum_{j=1}^{3} \sum_{\mathbf{k}} \exp^{i\mathbf{k}.\delta_j} a^{\dagger}_{-\mathbf{k}\downarrow} b^{\dagger}_{\mathbf{k}\uparrow} \\ \sum_{<i>\sigma} a^{\dagger}_{i\uparrow} b^{\dagger}_{j\downarrow} &= \sum_{\mathbf{k}} \phi(\mathbf{k}) a^{\dagger}_{-\mathbf{k}\downarrow} b^{\dagger}_{\mathbf{k}\uparrow} \end{aligned} \tag{4.23}$$

where

$$\sum_{\mathbf{k}} \sum_{j=1}^{3} \exp^{i\mathbf{k}.\delta_j} = \phi(\mathbf{k}) \tag{4.24}$$

Hence, considering all the terms as shown above, we can write the total Hamiltonian as

$$\begin{aligned} H &= -t[\phi(\mathbf{k}) a^{\dagger}_{\mathbf{k}\sigma} b_{\mathbf{k}\sigma} + \phi(\mathbf{k}) b^{\dagger}_{\mathbf{k}\sigma} a_{\mathbf{k}\sigma}] - \mu[a^{\dagger}_{\mathbf{k}\sigma} a_{\mathbf{k}\sigma} + b^{\dagger}_{\mathbf{k}\sigma} b_{\mathbf{k}\sigma}] \\ &\quad + \sum_{\mathbf{k}} g_0 \Delta_0 (a^{\dagger}_{\mathbf{k}\uparrow} a^{\dagger}_{-\mathbf{k}\downarrow} + b^{\dagger}_{\mathbf{k}\uparrow} b_{-\mathbf{k}\downarrow}) + h.c. \\ &\quad + \sum_{\mathbf{k}} g_1 \Delta_1 (a^{\dagger}_{\mathbf{k}\uparrow} b^{\dagger}_{-\mathbf{k}\downarrow} + b^{\dagger}_{-\mathbf{k}\uparrow} a^{\dagger}_{\mathbf{k}\downarrow}) + h.c. + E_0 \end{aligned} \tag{4.25}$$

Noting that in the space of the moments Δ_1 is written by:

$$\Delta_{\mathbf{k}} = \sum_{ij} \Delta_{1,ij} \exp^{-\mathbf{k}.(\mathbf{r}_i - \mathbf{r}_j)} = \Delta_1 \phi(\mathbf{k})$$

And, for first order approximation in $\mathbf{k}$ next to Dirac points in $\mathbf{Q}_0$ [4], $\Delta_{\mathbf{k}}$ is rewritten as:

$$\Delta_{\mathbf{Q_0}+\mathbf{k}} = (3a/2)\Delta_1 (k_x + ik_y)$$

We then have the symmetry of the exotic wave p + ip in terms of the number of waves, see Fig. 4.1.

4.2 Methodology

The superconductivity in graphene can be studied in details using the expression of the Hamiltonian H. It consists of a hopping term relevant for the two sublattices of graphene resembling the kinetic energy part of the Hamiltonian. The chemical potential energy term is important to consider the zero of the kinetic energy to be μ. In neutral graphene the chemical potential crosses exactly through the Dirac point ($\mu = 0$). Moreover, the pairing terms involve the electron-electron interactions. The Hamiltonian can be diagonalized in the Nambu basis $\Psi_{\mathbf{k}} = (a_{\mathbf{k}\uparrow}, b_{\mathbf{k}\uparrow}, a^{\dagger}_{-\mathbf{k}\downarrow} b^{\dagger}_{-\mathbf{k}\downarrow})$ as shown earlier. Therefore, writing the Hamiltonian in matricial form,

$$\widehat{H} = \begin{bmatrix} -\mu & -t\phi_{\mathbf{k}} & g_0\Delta_0 & g_1\Delta_{1,\mathbf{k}} \\ t\phi^*_{\mathbf{k}} & -\mu & g_1\Delta_{1,-\mathbf{k}} & g_0\Delta_0 \\ g_0\Delta_0 & g_1\Delta_{1,-\mathbf{k}} & \mu & t\phi_{\mathbf{k}} \\ g_1\Delta_{1,\mathbf{k}} & g_0\Delta_0 & t\phi^*_{\mathbf{k}} & \mu \end{bmatrix} \tag{4.26}$$

and utilizing the the secular equation $det(H - EI) = 0$, we can obtain the eigenvalues and eigenvectors needed for further study. Hence,

$$\det \begin{bmatrix} -\mu - E & -t\phi_{\mathbf{k}} & g_0\Delta_0 & g_1\Delta_{1,\mathbf{k}} \\ t\phi^*_{\mathbf{k}} & -\mu - E & g_1\Delta_{1,-\mathbf{k}} & g_0\Delta_0 \\ g_0\Delta_0 & g_1\Delta_{1,-\mathbf{k}} & \mu - E & t\phi_{\mathbf{k}} \\ g_1\Delta_{1,\mathbf{k}} & g_0\Delta_0 & t\phi^*_{\mathbf{k}} & \mu - E \end{bmatrix} = 0 \tag{4.27}$$

The eigen values are given by,

$$E_{\mathbf{k}s} = \pm\sqrt{(t \mid \phi_{\mathbf{k}} \mid +s\mu)^2 + (g_0\Delta_0 + sg_1\Delta_1 \mid \phi_{\mathbf{k}} \mid)^2} \tag{4.28}$$

where $s = \pm 1$ and $E_{\mathbf{k}\alpha s} \equiv E_{\mathbf{k}s}$ where $\alpha = \pm 1$, so we have the eigen-energies as: $E_{\mathbf{k}++}, E_{\mathbf{k}-+}, E_{\mathbf{k}+-}, E_{\mathbf{k}--}$.

So, the Hamiltonian can be diagonalized and rewritten as:

$$H = \sum_{\mathbf{k}\alpha s} E_{\mathbf{k}\alpha s} n^B_{\mathbf{k}\alpha s} + E_0$$

The self consistent equations for calculation of the superconducting gap parameters and also its temperature dependencies can be obtained from the free energy (F) expression. Now the two mean-field equations can be obtained by the stationary condition of F with respect to the corresponding order parameters $\partial F/\partial\Delta_0$, $\partial F/\partial\Delta_1$. The free energy of graphene is given by

$$F = -\frac{1}{\beta}\sum_{\mathbf{k},\alpha,s} \ln(1 + e^{-\beta E_{\mathbf{k}\alpha s}}) + E_0 \tag{4.29}$$

where we have $\beta = \frac{1}{k_B T}$.Considering the four eigenvalues $E_{\mathbf{k}-+} = -E_{\mathbf{k}++}$ e $E_{\mathbf{k}--} = -E_{\mathbf{k}+-}$ of the Hamiltonian we can simplify the free energy and write it as

$$F = -\frac{1}{\beta}\sum_{\mathbf{k}s} 2\ln\left(2\cosh\frac{E_{\mathbf{k}\alpha}}{2T}\right) + E_0 \tag{4.30}$$

The derivative of the energies are:

$$\frac{dE_{k+}}{d\Delta_0} = \frac{1}{2E_{k+}}(2g_0^2\Delta_0 + 2g_0g_1\Delta_1 \mid \phi_k \mid)$$

$$\frac{dE_{k-}}{d\Delta_0} = \frac{1}{2E_{k-}}(2g_0^2\Delta_0 - 2g_0g_1\Delta_1 \mid \phi_k \mid)$$

$$\frac{dE_{k+}}{d\Delta_1} = \frac{1}{2E_{k+}}(2g_1^2\Delta_1 \mid \phi_k \mid^2 + 2g_0g_1\Delta_0 \mid \phi_k \mid)$$

$$\frac{dE_{k-}}{d\Delta_1} = \frac{1}{2E_{k-}}(2g_1^2\Delta_1 \mid \phi_k \mid^2 - 2g_0g_1\Delta_0 \mid \phi_k \mid)$$

The resulting two equations for the gaps Δ_0 and Δ_1 are written. Thus the of self-consistent equations are:

$$\Delta_0 = -\frac{1}{2}\sum_{\mathbf{k},s}\frac{(g_0\Delta_0 + sg_1\Delta_1 \mid \phi_{\mathbf{k}} \mid)}{E_{\mathbf{k},s}}\tanh\left(\frac{E_{\mathbf{k}s}}{2T}\right) \tag{4.31}$$

$$\Delta_1 = -\frac{1}{6}\sum_{\mathbf{k},s}\frac{\mid \phi_{\mathbf{k}} \mid (g_1\Delta_1 \mid \phi_{\mathbf{k}} \mid + sg_0\Delta_0)}{E_{\mathbf{k}s}}\tanh\left(\frac{E_{\mathbf{k,s}}}{2T}\right) \tag{4.32}$$

The above two equations can be solved numerically to obtain the gap values at $T = 0$. Varying the temperature, we shall also the temperature dependencies of the two order-parameters and also the value of the critical temperature of the system where the second order-phase transition is observed for graphene. Moreover, the temperature dependencies also allows us to calculate the thermodynamic parameters of the system like entropy, specific heat, internal energy and also the free energy. In the next section we shall discuss in details the dependencies and also calculate the specific heat of graphene.

4.3 Results and Discussion

In this section we would like to firstly consider the nature of the spectrum obtained from the pairing Hamiltonian of graphene. Secondly a numerical calculation of the model should be performed in detail to understand superconducting nature of graphene. The spectrum energy

is given by the equation.

$$E_{\mathbf{k}s} = \pm\sqrt{(t \mid \phi_{\mathbf{k}} \mid +s\mu)^2 + (g_0\Delta_0 + sg_1\Delta_1 \mid \phi_{\mathbf{k}} \mid)^2} \tag{4.33}$$

In the s wave state where $\Delta_0 \neq 0$ and $\Delta_1 = 0$ e $\mu \neq 0$, the spectrum is given by $E_{\mathbf{k}s} = \pm\sqrt{(t \mid \phi_{\mathbf{k}} \mid +s\mu)^2 + (g_0\Delta_0)^2}$ and the gap energy of the s-wave is given by $E_g^{(0)} = 2g_0\Delta_0$. On the other hand for the $p+ip$ state when we have $\Delta_0 = 0$, $\Delta_1 \neq 0$ e $\mu \neq 0$, the order parameters of the p wave is given by:

$$E_g^{(1)} = 2 \mid \mu g_1\Delta_1 \mid /\sqrt{t^2 + g_1^2\Delta_1^2} \tag{4.34}$$

where we observe a linear dependence on chemical potential. Varying the chemical potential we are able to study the system with doping. For $\Delta_0 = 0$, $\Delta_1 \neq 0$ e $\mu = 0$, we can write

$$E_{\mathbf{k}s} \;=\; \pm\sqrt{(t \mid \phi_{\mathbf{k}} \mid)^2 + (g_1\Delta_1)^2} \tag{4.35}$$

Defining an effective hopping parameter $t' = t\sqrt{1 + g_1\Delta_1^2/t^2}$, we get $E_{\mathbf{k}s} = t' \mid \phi_{\mathbf{k}} \mid$, thereby the effective hopping parameter renormalizes the Fermi-Dirac's velocity.

Let us consider the more general case where $\Delta_0 \neq 0$, $\Delta_1 \neq 0$ e $\mu \neq 0$, we have the presence of the both the gaps of s and $p+ip$ symmetries and the gap is given in terms of the parameter t as

$$E_g^{(0,1)} = 2\frac{\mid tg_0\Delta_0 - g_1\mu\Delta_1 \mid}{t'} \tag{4.36}$$

The mean-field phase diagram of graphene has been studied with μ [11] which demonstrates the three distinct phases depending on the interaction parameter: (i) s-wave phase for attractive values of the on-site interaction ($g_0 < 0$) and repulsive nearest neighbor interaction ($g_1 > 0$). (ii) $p+ip$ -wave phase for attractive nearest neighbor interaction ($g_1 < 0$) and repulsive on-site interaction ($g_0 > 0$) (iii) a coexistence phase of s and $p+ip$ phase for attractive values of the on-site interaction ($g_0 < 0$) and nearest neighbor interaction ($g_1 < 0$). As we know that the physical realization of superconductivity is difficult we can obtain superconductivity on doping the material that shifts the chemical potential values to values away from the Dirac point. This could be possible for e.g by chemically doping graphene with a metal. Hence to understand the superconductivity caused by doping in graphene we consider the phase that has coexistence of the two gaps for $\mu > 0$.

The self-consistent equations obtained previously was numerically solved to obtain the values of the order parameters and their dependencies on temperature. All our results in this work are in units of t unless mentioned otherwise. The parameters utilized in our work were chosen as per ref. [11] and also in accordance with the experimental values of graphene. In Fig. (4.4) we plot the temperature dependencies of the order parameters Δ_0 and Δ_1. The figure exhibits three different sets of the interaction parameters: $g_0 = -0.15$, $g_1 = -0.1$ (blue solid line) , $g_0 = -0.2$, $g_1 = -0.1$ (black solid line) and $g_0 = -0.25$, $g_1 = -0.1$ (red solid line). The chemical potential value for the above sets of calculation were chosen to be $\mu = -0.1$. The

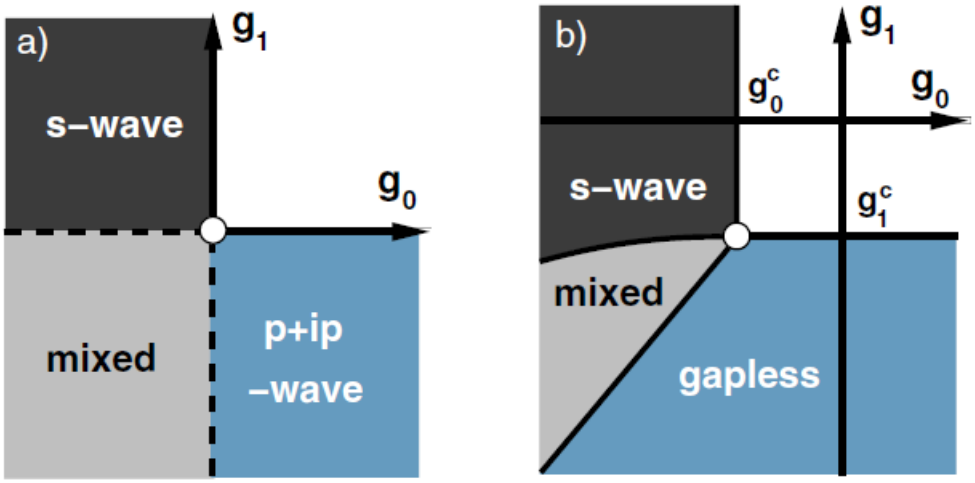

Figure 4.3: Mean field phase diagram [13].

higher value of the gap parameter represents the s-wave whereas the lower value is for the $p+ip$ symmetry. The coexistence of the order parameters is observed for all temperatures below the critical temperature. Moreover, Δ_0 is always larger than Δ_1 for all T. As the on-site interaction g_0 increase we observe a rise in the T_c values. For ($g_0 = -0.15$, $g_1 = -0.1$), T_C is 4.8k, whereas for ($g_0 = -0.2$, $g_1 = -0.1$), $T_c = 12.4$k and for ($g_0 = -0.25$,$g_1 = -0.1$), $T_c = 25$k.

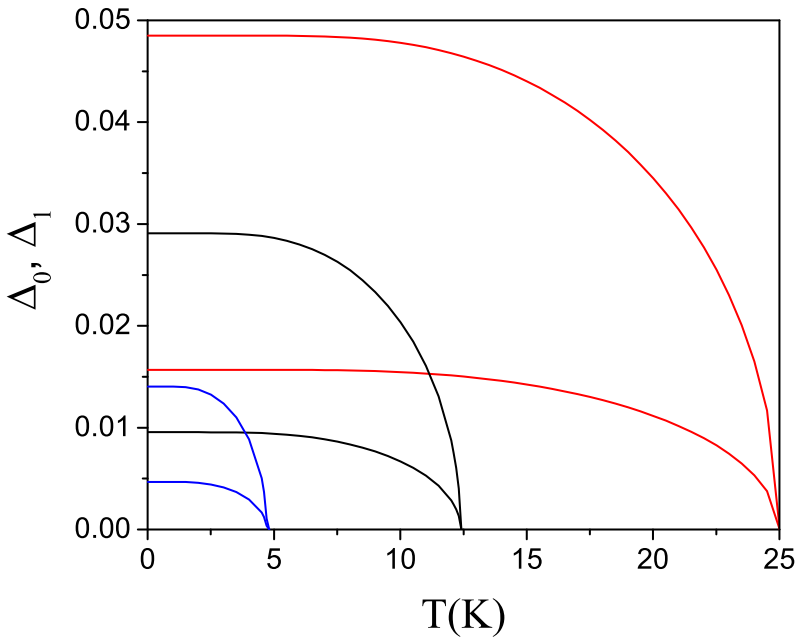

Figure 4.4: Δ_0 ,Δ_1 vs T for $g_0 = -0.15$,$g_1 = -0.1$ (blue solid line), $g_0 = -0.2$,$g_1 = -0.1$(black solid line) and $g_0 = -0.25$,$g_1 = -0.1$ (red solid line) and $\mu = -1.0$.

Fig. (4.5) exhibit the temperature dependencies of Δ_0 and Δ_1 with various values of the nearest-neighbor interaction. The figure exhibits three different sets of the interaction param-

eters: ($g_0 = -0.2$,$g_1 = -0.05$ (blue solid line) , $g_0 = -0.2$, $g_1 = -0.1$(black solid line) and $g_0 = -0.2$, $g_1 = -0.15$ (red solid line). The higher value of the gap parameter represents the s-wave whereas the lower value is for the $p + ip$ symmetry. We observe a similar trend and qualitative behavior as compared to Fig. (4.4), where we have a unique critical temperature and the gap values increases with the increase in g_1. As the nearest-neighbor interaction g_1 increase we observe a rise in the T_c values. For ($g_0 = -0.2$,$g_1 = -0.05$), T_C is 9.5k, whereas for $g_0 = -0.2$,$g_1 = -0.1$, $T_c = 12,4$k and for ($g_0 = -0.2$, $g_1 = -0,15$), $T_c = 16.0$k. The figure demonstrates that the on-site interaction has a larger effect on the critical temperature values of graphene.

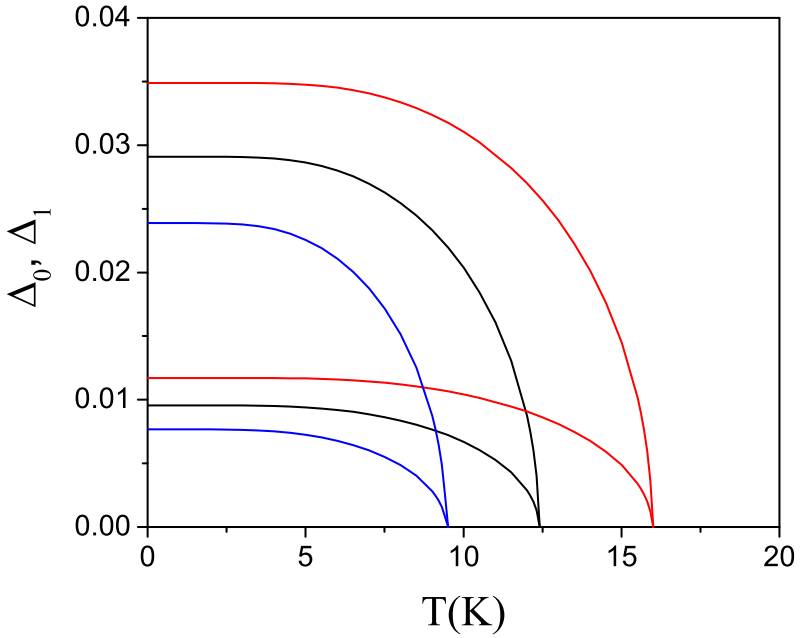

Figure 4.5: Δ_0, Δ_1 vs T for $g_0 = -0.2$, $g_1 = -0.05$ (blue solid line), $g_0 = -0.2$,$g_1 = -0.1$ (black solid line), $g_0 = -0.2$, $g_1 = -0.15$ (red solid line) and $\mu = -1.0$..

In Fig. (4.6), the dependence of the order parameters on chemical potential was studied. The dependencies were studied for the interaction parameters $g_0 = -0,2, g_1 = -0,1$ for three values of μ: $\mu = -1.0$ (red solid line), $\mu = -1.1$ (black solid line), $\mu = -1.2$ (blue solid line). The critical temperatures for $\mu = -1.0$, -1.1 and -1.2 are $16K$, 7k and 4.6k , respectively. The higher value of the gap parameter represents the s-wave whereas the lower value is for the $p+ip$ symmetry. As we increase doping we observe a decrease in the critical temperature of graphene. With further increase in μ, superconductivity in graphene should disappear completely.

Next, the normalized order parameters $\Delta_0(T)/\Delta_0(T_c)$ and $\Delta_1(T)/\Delta_1(T_c)$ are plotted vs the normalized temperature (T/T_c) for $g_0 = -0.2$, $g_1 = -0.15$ for $\mu = -1.0$, -1.1 and -1.2. It also includes form$g_0 = -0.2$, $g_1 = -0.1$ for $\mu = -1.0$, -1.1 and -1.2. An universal character of the parameters is observed for both type of order parameters irrespective of the interaction strength and doping of graphene. It also resembles the characteristic curve of the BCS theory

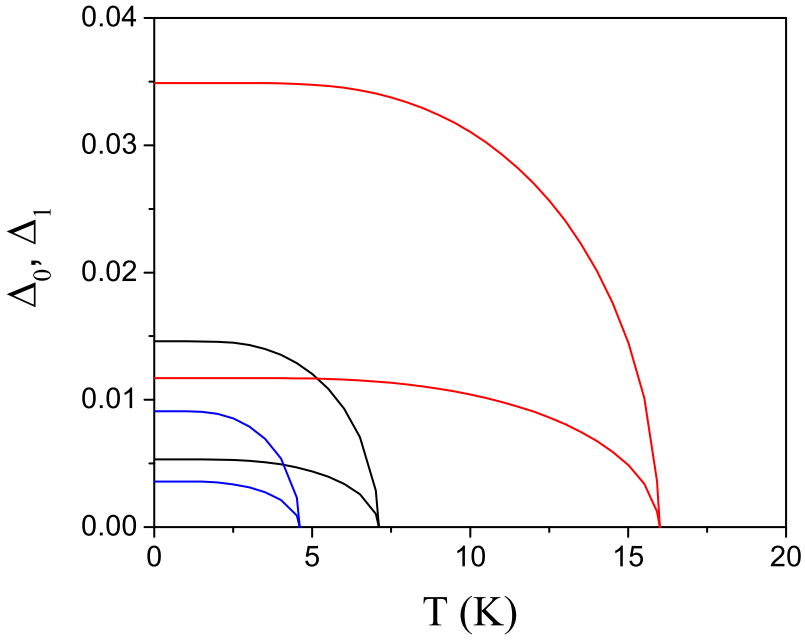

Figure 4.6: Δ_0, Δ_1 vs μ for $g_0 = -0.2$, $g_1 = -0.15$ and$\mu = -1.0$ (red solid line), $\mu = -1.1$ (black solid line), $\mu = -1.2$ (blue solid line) .

[10].

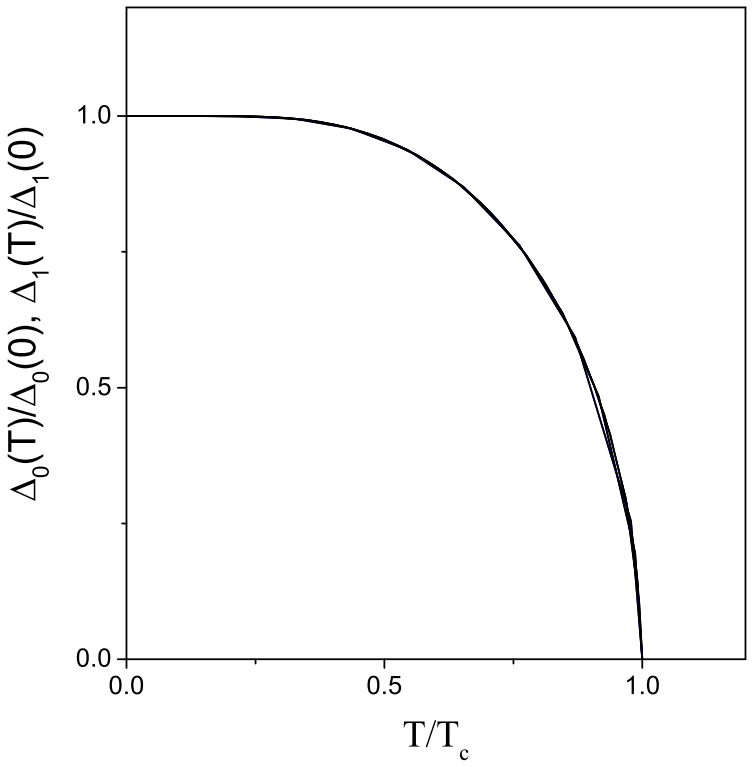

Figure 4.7: $\Delta_0(T)/\Delta_0(T_c)$ and $\Delta_1(T)/\Delta_1(T_c)$ are plotted vs the normalized temperature (T/T_c).

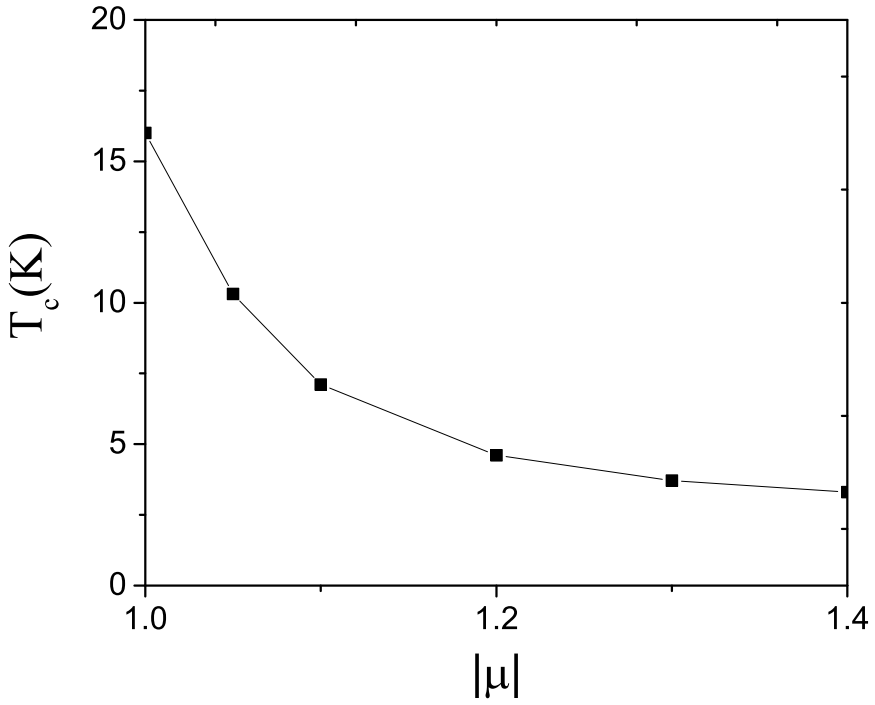

Figure 4.8: Critical temperature vs $|\mu|$ for $g_0 = 0.2$ and $g_1 = 0.15$.

The dependence of the critical temperature of graphene [11] on interaction is generally given by the following expression:

$$T_C \approx 2\mu(\gamma/\pi)exp(-\Lambda(g_0^c/g_0 - 1)\mu^{-1} - 1) \tag{4.37}$$

where γ is Euler's constant. Hence we should expect that the critical temperature drops exponentially with the chemical potential and should tend to saturate for higher values of potential. In Fig. (4.8) we plot the critical temperature vs $|\mu|$ for $g_0 = 0.2$ and $g_1 = 0.15$. We observe that the critical temperature decreases exponentially with $|\mu|$ initially and tends then to saturate for higher values of the chemical potential until it vanishes completely for high values of the chemical potential. In Figs. (4.9) and (4.10) the dependence of T_c on the interaction parameter $\mid g_0 \mid$ and $\mid g_1 \mid$ are considered. The line drawn has been provided as a guide to the eye for better observation. T_c increases with the increase in the interaction strengths. However, the dependence of T_c is more pronounced on $\mid g_0 \mid$, as was also observed earlier. The characteristics of superconductivity in graphene was observed from the graphs on the order parameters and the nature of the critical temperatures. The temperature dependencies of the order parameters allow us to calculate the thermodynamic properties of the system. Hence, in the following figure we demonstrate the temperature dependence of electronic specific heat of the system. The general equation for specific heat is:

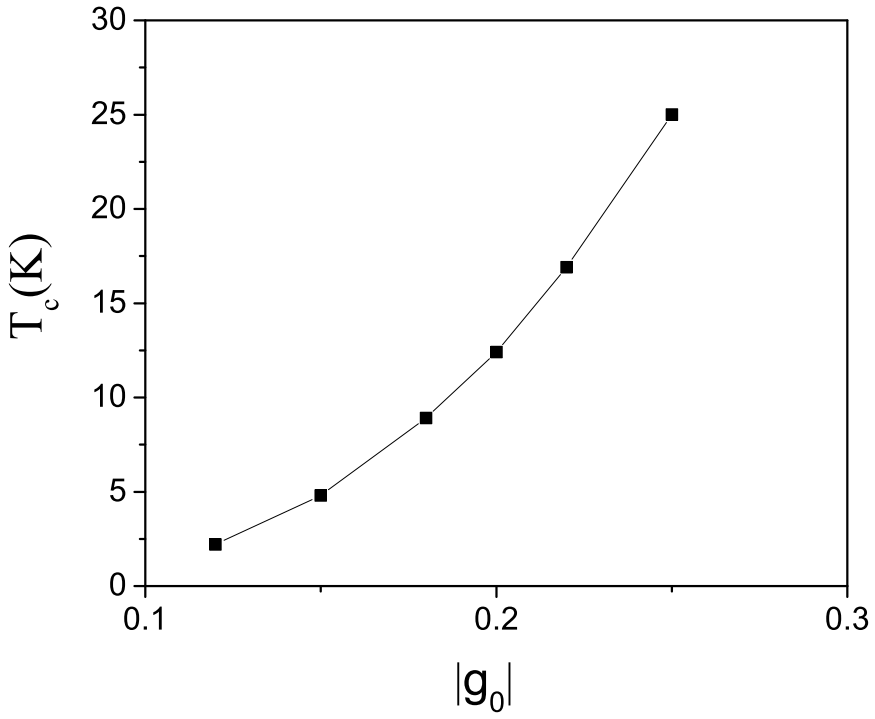

Figure 4.9: Critical temperature vs $|g_0|$ for $\mu = -1.0$ and $g_1 = -0.1$.

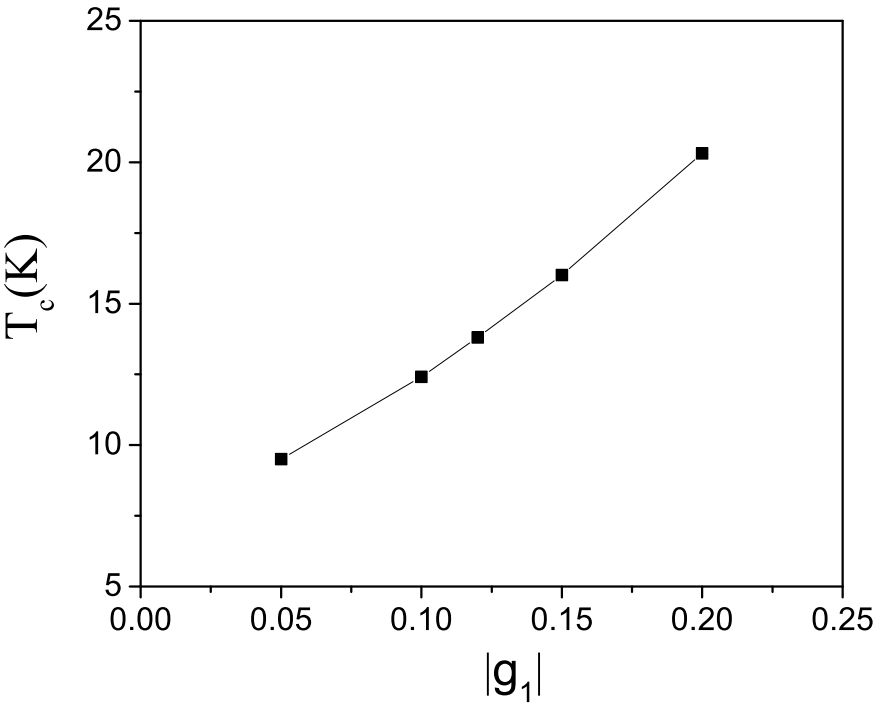

Figure 4.10: Critical temperature vs $|g_1|$ for $\mu = -1.0$ and $g_0 = -0.2$.

$$\begin{aligned} C_s &= 2\beta k_B \sum_{\mathbf{k}\alpha} -\frac{\partial f^{\alpha}_{\mathbf{k}}}{\partial E^{(\alpha)}_{\mathbf{k}}} \left(E^{(\alpha)2}_{\mathbf{k}} + \frac{1}{2}\beta E^{(\alpha)}_{\mathbf{k}} \frac{dE^{(\alpha)}_{\mathbf{k}}}{d\beta} \right) \\ &= 2\beta^2 k_B \sum_{\mathbf{k}\alpha} f^{\alpha}_{\mathbf{k}}(1 - f^{\alpha}_{\mathbf{k}}) \left[E^{(\alpha)2}_{\mathbf{k}} + \frac{T}{2} \left(-g_0^2 \frac{d\Delta_0^2}{dT} - g_1^2 |\phi_{\mathbf{k}}|^2 \frac{d\Delta_1^2}{dT} \pm 2g_1 |\phi_{\mathbf{k}}| \frac{d\Delta_1 \Delta_0}{dT} \right) \right] \end{aligned} \quad (4.38)$$

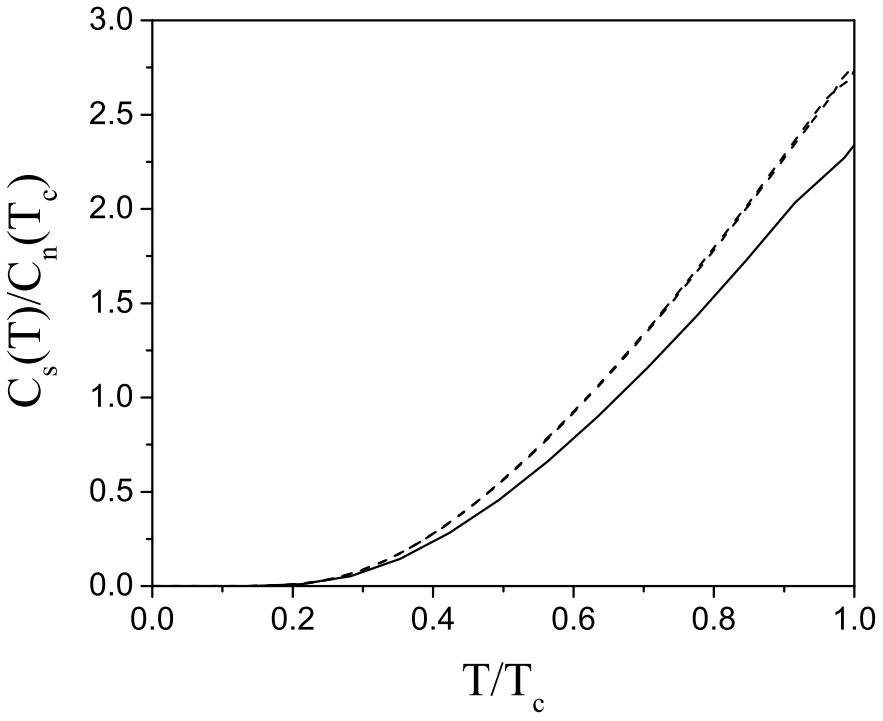

Figure 4.11: Specific heat $C_s(T)/C_n(T_c)$ vs T/T_c for $g_0 = 0.2$, $g_1 = 0.15$ $g_0 = 0.2$ and $g_1 = 0.1$ for $\mu = -1.0$ (dashed line) and $\mu = -1.1$ (solid line).

where $\frac{d\Delta_0^2}{dT}$, $\frac{d\Delta_1^2}{dT}$ and $\frac{d\Delta_1\Delta_0}{dT}$ are the derivatives of the two types of gaps in the coexistence phase of graphene. Therefore, we have the specific superconducting heat in which the first time refers to the redistribution of particles and the second term is derived from the parameters of the order of waves s and p+ip. Figure (4.11) exhibits the specific heat vs temperature plot for $g_0 = 0.2$, $g_1 = 0.15$ $g_0 = 0.2$ and $g_1 = 0.1$ for $\mu = -1.0$ (dashed line) and $\mu = -1.1$ (solid line). The jump $\Delta C(T)/C_n(T_c)$ in the specific heat is seen to be dependent on μ. $\Delta C(T)/C_n(T_c)$ is found to be 1.34 for $\mu = -1.0$ and 1.73 for $\mu = -1.1$. It increases with the increase in μ denoting a rise in chemical doping of graphene. The above rise in the jump for specific heat with doping was also observed in ref. [59]. Moreover, it is to be noted that the jump in the BCS case is of the order of 1.43 [10]. Hence with doping we can surpass the jump in the specific heat for graphene.

Chapter 5

Conclusions

The main objective of this was to obtain the behavior of the order parameters, we specifically analyzed the mixed-phase wave for interaction of attractive origin, the critical temperatures and specific heat of the single layer superconducting state of graphene due to the doping as well as to evaluate the critical values for the transition from the superconducting state to the normal.

From the definitions of order parameters via mean field theory we obtained the s-wave and the exotic wave $p+ip$. Also,we got the eigen-energies and, consequently, the gap energies $E_g^{(0)}$, $E_g^{(1)}$ and $E_g^{(0,1)}$ were presented [13]. Minimization the free energy of the system resulted in self-consistent coupled equations.

The self-consistent equations were solved numerically to obtain the gap values at zero temperature. Order parameters (for attractive energies) coexisted at temperatures below T_C that vanishes simultaneously at the same critical temperature. Moreover, Δ_0 is always greater than Δ_1. As we increase doping, the critical temperature decreases. The graph of normalized order parameters is also presented. The universal characteristic of the parameters is observed and is found to be similar to the characteristic curve of the BCS theory.

Critical temperature drops exponentially with chemical potential and should tend to saturate for higher values of potential. The normalized specific heat dependence on temperature was obtained. The jump Δ_C exhibits similarity to the BCS theory and with the increase of μ, C_S also rises. Hence with doping we can surpass the jump in the specific heat for graphene.

We conclude that there is a direct influence of the doping of superconducting states in the single layer of graphene as observed in the dependencies of the order parameters, critical temperature and also in thermodynamic quantities. As a perspective, we intend to extend this research by increasing the amount of graphene layers in order to look for critical optimized values such as the rise in the critical temperature.

Bibliography

1 WALLACE, P. R. The band theory of graphite. **Physical Review**, v. 71, n. 9, p. 622–634, 1947.

2 TERRONES, M. Graphene and graphite nanoribbons: Morphology, properties, synthesis, defects and applications. **Nano today**, v. 5, p. 351–372, 2010.

3 CLAYDEN, J.; GREEVES, N.; WARREN, S. **Organic Chemistry**. [S.I.]: Oxford University Spress., 2012. v. 2. 86 p.

4 DARTORAL, C.; JIMENEZ, M. J. S.; ZANELLA, F. Os fundamentos da física dos féermions de dirac sem massa em (1+2)-d e o grafeno. **Revista Brasileira de Ensino de Física**, v. 37, n. 3301, p. 01–06, 2015.

5 NETO, A. H. C.; GUINEA, F.; PERES, N. M. R.; NOVOSELOV, K. S.; GEIM, A. K. The electronic properties of graphene. **Reviews of Modern Physics**, v. 81, p. 1103–1106, 2009.

6 ROSE-INNES, A. C.; RHODERICK, E. H. **Introduction to superconductivity**. [S.I.]: Oxford:Pergamon, 1978. v. 1ed. 237 p.

7 MOURACHKINE, A. **Room-Temperature superconductivity**. Cambridge: Cambridge International Science Publishing, 2004. 03–08 p.

8 COOPER, L. N.; FELDMAN, D. **BCS: 50 Years.** Singapore: World Scientific Publishing Co. Pte. Ltd., 2011. v. 1ed. 06 p.

9 GROSSO, G.; PARRAVICINI, G. P. **Solid State Physics**. [S.I]: Academic Press, 2013. 673 p.

10 TINKHAM, M. **introduction to superconductivity**. New York: McGraw-Hill, Inc., 2004. 43–66 p.

11 NETO, A. H. C. Charge density wave, superconductivity, and anomalous metallic behavior in 2d transition metal dichalcogenides. **Physical Review Letters**, v. 86, n. 4238, p. 01–04, 2001.

12 SIVABRATA, S.; ROUT, G. C. Band gap opening in graphene: a short theoretical study. **Nano Letters**, v. 07, p. 81–89, 2017.

13 UCHOA, B.; NETO, A. H. C. Superconducting states of pure and doped graphene. **Physical Review Letters**, v. 98, n. 46801, p. 01–04, 2007.

14 SCHWIERZ, F. Industry-compatible graphene transistors. **Nature**, v. 472, p. 41–42, 2011.

15 SUVARNAPHAET, P.; PECHPRASARN, S. Graphene-based materials for biosensors: A review. **Multidisciplinary Digital Publishing Institute**, v. 17, n. 2061, p. 01–16, 2017.

16 KOTOV, V. N.; UCHOA, B.; PEREIRA, V. M.; GUINEA, F.; NETO, A. H. C. Electron-electron interactions in graphene: Current status and perspectives. **Review of Modern Physics**, v. 84, p. 110–113, 2012.

17 BERNAL, J. B. The structure of graphite. **Proceedings of the Royal Society of London**, v. 472, p. 749–773, 1924.

18 NOVOZELOV, K. S.; GEIM, A. K.; S.V.MOROZOV; JIANG, D.; ZHANG, Y.; DUBONOS, S.; I.V.GRIGORIEVA; FIRSOV, A. Electric field effect in atomically thin carbon films. **Science**, v. 22, p. 666–669, 2004.

19 SHANKER, V.; BHARGAVA, S. K.; JANPAIAH, D.; MANCHALA, S. Novel and highly efficient strategy for the green synthesis of soluble graphene by aqueous polyphenol extracts of eucalyptus bark and its applications in high-performance supercapacitors. **ACS Publications research**, v. 7, p. 11612–11620, 2009.

20 SALUNKE, B. K.; KIM, B. S. Facile synthesis of graphene using a biological method. **RSC Advances**, v. 506, n. 06, p. 17158–17162, 2020.

21 LIMA, B.; BERNARDI, M.; MASTELARO, V. Wavelength effect of ns-pulsed radiation on the reduction of graphene oxide. **Applied Surface Science**, v. 506, n. 144808, p. 01–06, 2020.

22 DALE, E. P. R.; BROWNSON, A. C.; BANKS, C. E. A decade of graphene research: production, applications and outlook. **Materials today**, v. 17, p. 426–432, 2014.

23 LIAO, L.; LIN, Y.-C.; BAO, M.; CHENG, R.; BAI, J.; LIU, Y.; QU, Y.; WANG, K. L.; HUANG, Y.; DUAN, X. High-speed graphene transistors with a self-aligned nanowire gate. **Materials today**, v. 467, p. 305–308, 2010.

24 ZHUANG, X.; CHEN, Y.; LIU, G.; LI, P.; ZHU, C.; KANG, E.; NOEH, K.; ZHANG, B.; ZHU, J.; LI, Y. Conjugated-polymer-functionalized graphene oxide: Synthesis and nonvolatile rewritable memory effect. **Advanced Materials**, v. 22, p. 1731, 2010.

25 ZHANG, X.; ZHANG, X.; WANG, S.; LIU, M.; TAO, L.; ; WEI, Y. Surfactant modification of aggregation-induced emission material as biocompatible nanoparticles: Facile preparation and cell imaging. **Nanoscale**, v. 5, n. 4134, p. 147–150, 2012.

26 WANG, H.; SUN, K.; TAO, F.; STACCHIOLA, D. J.; HU, Y. H. 3d honeycomb-like structured graphene and its high efficiency as a counter-electrode catalyst for dye-sensitized solar cells. **Angewandte Chemie**, v. 52, p. 9210, 2013.

27 LIN, W.; LIAO, C.-S.; JHANG, J.-H.; TSAI, Y.-C. Graphene modified basal and edge plane pyrolytic graphite electrodes for electrocatalytic oxidation of hydrogen peroxide and β-nicotinamide adenine dinucleotide. **Electrochemistry Communications**, v. 11, p. 2153, 2009.

28 REICH, S.; MAULTZSCH, J.; ORDEJóN, P. Tight-binding description of graphene. **Physical Review B**, v. 66, n. 035412, p. 01–05, 2002.

29 DEACON, R. S.; CHUNG, K. C.; NOVOSELOV, K. S. Cyclotron resonance study of the electron and hole velocity in graphene monolayers. **Physical Review B**, v. 76, n. 081406(R), p. 01–03, 2007.

30 SIMON, S. H. **The Oxford Solid State Basics**. Oxford: Oxford University Press, 2013. v. 1ed. 19–34 p.

31 GENNES, P. G. **Superconductivity of Metals and Alloys**. New York: CRC Press Taylor & Francis Group, 2018. 93–96 p.

32 MEISSNER, W.; OCHSENFELD, R. **Ein neuer Effekt bei Eintritt der Supraleitfähigkeit**. [S.I.]: The Science of Nature, 1933. 787 p.

33 COPPER and Electricity: Generation. <https://copperalliance.org.uk/knowledge-base/education/education-resources/copper-electricity-generation/>. 'Acessado em 05/06/2021',.

34 WANG, X.; GOURLAY, S. A.; PRESTEMON, S. O. Dipole magnets above 20 tesla: Research needs for a path via high-temperature superconducting rebco conductors. **MDPI.**, p. 04, 2019.

35 KIRTLEY, J. R.; KETCHEN, M.; STAWIASZ, K. G.; SUN, J. Z.; GALLAGHER, W. J.; BLANTON, S. H.; WIND, S. J. High-resolution scanning squid microscope. **American Institute of Physics.**, p. 01–03, 1995.

36 LONDON, F.; LONDON, H. The electromagnetic equations of the supraconductor. **Proceedings of the Royal Society A: Mathematical, Physical and Engineering Sciences**, v. 149, p. 71–88, 1935.

37 CYROT, M. Ginzburg-landau theory for superconductors. **Reports on Progress in Physics**, p. 103–158, 1973.

38 SCHIEFFER, J. R. **Theory of Superconductivity**. New York: CRC Press Taylor & Francis Group, 2018. 25–56 p.

39 COOPER, L. L. Bound electron pairs in a degenerate fermi gas. **Physical Review**, v. 104, n. 4, p. 1189–1190, 1956.

40 POOLER, C. P. **Handbook of superconductivity.** San Diego: Academic press, 2000. v. 1ed. 58–61 p.

41 HEERSCHE, H. B.; HERRERO, P. J.; OOSTINGA, J. B.; VERSYPEN, L. K.; MORPURGO, A. Bipolar supercurrent in graphene. **Nature(London).**, p. 55–56, 2007.

42 MIAO, F.; WIJERATNE, S.; ZHANG, Y.; COSKUN, U. C.; BAO, W.; N.LAU, C. Phase-coherent transport in graphene quantum billiards. **Science.**, v. 317, p. 1530–1533, 2007.

43 ARISTIZABAL, C. O.; FERRIER, M.; GUéRON, S.; BOUCHIAT, H. Tuning the proximity effect in a superconductor-graphene-superconductor junction. **Physical Review B**, v. 79, p. 165436, 2009.

44 BEENAKKER, C. W. J. Specular andreev reflection in graphene. **Physical Review Letters**, v. 97, p. 067007, 2006.

45 BLACK-SCHAFFER, A. M.; DONIACH, S. Self-consistent solution for proximity effect and josephson current in ballistic graphene sns josephson junctions. **Physical Review B**, v. 78, p. 024504, 2008.

46 BERGMAN, D.; HUR, K. L. Near-zero modes in condensate phases of the dirac theory on the honeycomb lattice. **Physical Review B**, v. 79, p. 185420, 2009.

47 LINDER, J.; YOKOYAMA, T.; HUERTAS-HERNO, D.; SUDBO, A. Supercorrent switch in graphene π junctions. **Physical Review Letters.**, v. 100, p. 187004, 2008.

48 GREENBAUM, D.; DAS, S.; SCHWIETE, G.; SILVESTROV, P. G. Pure spin current in graphene normal-superconductor structures. **Physical Review B.**, v. 75, p. 195437, 2007.

49 HANNAY, N. B.; GABALLE, T. H.; MATTHIAS, B. T.; ANDRES, K.; SCHIMIDTAND, P.; MACNAIR, D. Superconductivity in graphitic compounds. **Physical Review B**, v. 14, p. 225, 1965.

50 CSANYI, G.; LITTLEWOOD, P. B.; NEVIDOMSKYY, A. H.; D.SIMONS, C. P. B. The role of the interlayer state in the electronic structure of superconducting graphite intercalated compounds. **Nature Physics**, v. 1,42, p. 42, 2005.

51 GONZALEZ, J. Behavior of ϕ^4 kinks in the presence of external forces. **Physical Review B**, v. 45, p. 10338, 1992.

52 HONERKAMP, C. Density waves and cooper pairing on the honeycomb lattice. **Physical Review Letters**, v. 100, p. 146404, 2008.

53 PATHAK, S.; SHENOY, V. B.; BASKARAN, G. Possible high-temperature superconducting state with a d+id pairing symmetry in doped graphene. **Physical Review B**, v. 81, p. 085431, 2010.

54 FORTI, S.; EMTSEV, K. V.; COLETTI, C.; ZAKHAROV, A.; RIEDL, C.; STARKE, U. Ambipolar doping in quasifree epitaxial graphene on sic (0001) controlled by ge intercalation. **Physical Review B**, v. 84, p. 125449, 2011.

55 PARK, C. H.; GIUSTINO, F.; COHEN, M.; LOUIE, S. Electron phonon interactions in graphene and bilayer graphene and graphite. **Nano Letters**, v. 84, p. 229, 2008.

56 MARGINE, E. R.; GIUSTINO, F. Two-gap superconductivity in heavily n doped graphene: Ab initio migdal-eliashberg theory. **Physical Review B**, v. 90, p. 014518, 2014.

57 SI, C.; LIU, Z.; DUAN, W.; LIU, F. First-principles calculations on the effect of doping and biaxial tensile strain on electron-phonon coupling in graphene. **Physical Review Letters**, v. 111, p. 196802, 2013.

58 SAVINI, G.; C., A. F.; GIUSTINO, F. First-principles prediction of doped graphane as a high-temperature electron-phonon superconductor. **Physical Review Letters**, v. 105, p. 037002, 2010.

59 DURAJSKI, A. P. Influence of hole doping on the superconducting state in graphane. **Superconductor Science and Tecnology**, v. 28, p. 035002, 2015.

60 MAHAN, G. D. **Many-Particle Physics**. New York: Physics of solids and liquids, 2000. v. 3ed. 23–31 p.

61 BRUSS, H.; FLENSBERG, K. **Many-body quantum theory in condensed matter physics**. Copenhagen: Orsted Laboratory, Niels Born Institute, University of Copenhagen, Mikroeletronik Centret, Techical University of Denmark, 2002. 65–68 p.

Appendix A

Comutation and anti-comutation between fermionic creation and destruction operators.

The wave function of anti-symmetric N-particles in the first quantization is generally written by the Slater determinant, as follows:

$$\mid \psi >= \frac{1}{\sqrt{N}} \begin{vmatrix} \phi_1(r_1) & \phi_1(r_2) & ... & \phi_1(r_N) \\ \phi_2(r_1) & \phi_2(r_2) & ... & \phi_2(r_N) \\ \vdots & \vdots & \ddots & \vdots \\ \phi_N(r1) & \phi_N(r2) & ... & \phi_N(r_N) \end{vmatrix}$$

where $\phi_N(r_N)$ represents the Nth atom in position N.

On the other hand, an ingenious way to rewrite fermions is through the description of the number of occupation of these particles. Thus $\mid n_{\mathbf{k}} >$ for the number of occupation of N particles and knowing that the fermions obey the Pauli principle of exclusion, which states that two identical fermions are not allowed (with the same quantum numbers) to occupy the same state and therefore $n_{\mathbf{k}} = 0, 1$, where $\mid 0 >$ represents the unoccupied state and $\mid 1 >$ the occupied state. In general denoted by:

$$\mid 0 >= \mid 0, ..., 0, \underbrace{0}_{\mathbf{k}}, ..., \underbrace{0}_{\mathbf{k'}}, 0, ... > \tag{A.1}$$

In the states $\mathbf{k}$ and $\mathbf{k}$'.

Denoting $c^{\dagger}_{\mathbf{k}}$ e $c_{\mathbf{k}}$ for the creation and destruction operators, respectively, of a fermion in the state $\mathbf{k}$, we get, $c^{\dagger}_{\mathbf{k}} \mid 1\rangle = 0$, $c_{\mathbf{k}} \mid 1\rangle = 0$ e $c_{\mathbf{k}} \mid 0\rangle = 0$. So we have the number operator $c^{\dagger}_{\mathbf{k}} c_{\mathbf{k}}$:

$$c^{\dagger}_{\mathbf{k}} c_{\mathbf{k}} \mid n_{\mathbf{k}}\rangle = n_{\mathbf{k}} \mid n_{\mathbf{k}}\rangle \tag{A.2}$$

where $n_{\mathbf{k}} = 0, 1$.

$$c^{\dagger}_{\mathbf{k}'} \mid 0 >= \mid 0 >= \mid 0, ..., 0, \underbrace{0}_{\mathbf{k}}, ..., \underbrace{1}_{\mathbf{k}'}, 0, ... > \tag{A.3}$$

$$c^{\dagger}_{\mathbf{k}} c^{\dagger}_{\mathbf{k}'} \mid 0 >= \mid 0 >= \mid 0, ..., 0, \underbrace{1}_{\mathbf{k}}, ..., \underbrace{1}_{\mathbf{k}'}, 0, ... > \tag{A.4}$$

Let us consider the operators in the reverse order and we get,

$$c^{\dagger}_{\mathbf{k}} \mid 0 >= - \mid 0 >= \mid 0, ..., 0, \underbrace{1}_{\mathbf{k}}, ..., \underbrace{0}_{\mathbf{k}'}, 0, ... > \tag{A.5}$$

$$c^{\dagger}_{\mathbf{k}'} c^{\dagger}_{\mathbf{k}} \mid 0 >= - \mid 0 >= \mid 0, ..., 0, \underbrace{1}_{\mathbf{k}}, ..., \underbrace{1}_{\mathbf{k}'}, 0, ... > \tag{A.6}$$

obeying the anti-symmetry of fermionic particles. Therefore:

$$(c^{\dagger}_{\mathbf{k}k'} c^{\dagger}_{\mathbf{k}} + c^{\dagger}_{\mathbf{k}} c^{\dagger}_{\mathbf{k}'}) = 0 \tag{A.7}$$

The commutation relations are

$$[c_{\vec{\mathbf{k}}\sigma}, c_{\vec{\mathbf{k}'}\sigma'}]_{+} = [c^{*}_{\vec{\mathbf{k}}\sigma}, c^{*}_{\vec{\mathbf{k}'}\sigma'}]_{+} = 0 \tag{A.8a}$$

$$[c_{\vec{\mathbf{k}}\sigma}, c^{*}_{\vec{\mathbf{k}'}\sigma'}]_{+} = \delta_{\vec{\mathbf{k}}\vec{\mathbf{k}'}} \delta_{\vec{\sigma}\vec{\sigma'}} \tag{A.8b}$$

$$c_{\vec{\mathbf{k}}\sigma}, c_{\vec{\mathbf{k}'}\sigma'+} = c^{*}_{\vec{\mathbf{k}}\sigma}, c^{*}_{\vec{\mathbf{k}'}\sigma'+} = 0 \tag{A.8c}$$

$$c_{\vec{\mathbf{k}}\sigma}, c^{*}_{\vec{\mathbf{k}'}\sigma'+} = \delta_{\vec{\mathbf{k}}\vec{\mathbf{k}'}} \delta_{\vec{\sigma}\vec{\sigma'}} \tag{A.8d}$$

Where σ e $\sigma^{'}$ represent the electron spins.

Appendix B

Tight Binding model.

B.1 Electrons in a periodic potential

Electrons placed in a potential $V(\mathbf{k})$ in which the periodicity is the same as $u_{\mathbf{k}n}(\mathbf{k})$ and its eigen-states of a periodic Hamiltonian are described by Bloch's states as we show bellow:

$$\psi_{\mathbf{k}n}(\mathbf{r}) = \exp^{i\mathbf{k}\cdot\mathbf{r}}\, u_{\mathbf{k}n}(\mathbf{k}) \tag{B.1}$$

$\mathbf{k}$ is the crystalline moment with $\mid \mathbf{k} \mid < k_F$ and n is the band index. Considering the bands are well separated, enough to use the local bands. The Hamiltonian in the space of the moment can be written as:

$$H = \sum_{\mathbf{k}\sigma} \epsilon_{\mathbf{k}} c^{\dagger}_{\mathbf{k}\sigma} c_{\mathbf{k}\sigma} \tag{B.2}$$

B.2 Wannier states

The name 'tight binding' suggests that this model of quantum mechanics describes the properties of electrons strongly bonded together in solids. The electrons in this model must be strongly bonded to the atom to which they belong and must have limited interaction with states and potentials in the surrounding atoms of the solid. Thus, the electron wave function becomes very similar to the atomic orbital of the free atom to which it belongs. The electron energy will also be close to the electron ionization energy in the free atom or ion because the interaction with potentials and states is limited. [60]

Let's assume that extension physics of the orbitals are smaller than the inter-atomic space. So we say that the orbitals are tightly connected in the network. The Wannier states located at $\mathbf{k}_i$ are defined as:

$$\mid \psi_i > = \frac{1}{\sqrt{N}} \sum_{\mathbf{k}} \exp^{-i\mathbf{k}\cdot\mathbf{R}_i} \mid \psi_{\mathbf{k}} > \tag{B.3}$$

We construct the states so that they are orthogonal to each other. Then:

$$\mid \mathbf{r} >= \sum_i < \psi_i \mid \mathbf{r} > \mid \psi_i > \tag{B.4}$$

We have

$$c_\sigma^\dagger(\mathbf{r}) = \psi_i^*(\mathbf{r}) c_{i\sigma}^\dagger \tag{B.5}$$

Similarly, inverting we have:

$$\mid c_{\mathbf{k}\sigma}^\dagger >= \frac{1}{\sqrt{N}} \sum_i \exp^{i\mathbf{k}\cdot\mathbf{R}_i} c_{i\sigma}^\dagger \tag{B.6}$$

So the Bloch Hamiltonian on that basis becomes:

$$H = \sum_{\mathbf{k}\sigma} \epsilon_{\mathbf{k}} c_{\mathbf{k}\sigma}^\dagger c_{\mathbf{k}\sigma} = \frac{1}{N} \sum_{ij} \sum_{\mathbf{k}\sigma} \exp^{i\mathbf{k}\cdot(\mathbf{R}_i - \mathbf{R}_j)} \epsilon_{\mathbf{k}} c_{i\sigma}^\dagger c_{j\sigma} \equiv \sum_{ij\sigma} t_{ij} c_{i\sigma}^\dagger c_{j\sigma} \tag{B.7}$$

Where $t_{ij} = \frac{1}{N} \sum_{\mathbf{k}} \exp^{i\mathbf{k}\cdot(\mathbf{R}_i - \mathbf{R}_j)} \epsilon_k$ is known as the Hopping Parameter for the electron to go from site i to site j.

B.3 Eletron-eletron interaction

We know that the term corresponding to the energy of interaction of two electrons at $\mathbf{r_i}$ e $\mathbf{r_j}$ is given by:

$$H_{e,e} = \frac{1}{2} \sum_{i \neq j} \frac{e^2}{\mid \mathbf{r_i} - \mathbf{r_j} \mid} \tag{B.8}$$

Using the basis of moments $\mid \mathbf{k}\sigma >$ and the free particle wave function :

$$\psi_{\mathbf{k},\sigma}(\mathbf{r}) =< \mathbf{r} \mid \mathbf{k}, \sigma >= \frac{1}{\sqrt{\nu}} \exp^{i\mathbf{k}\cdot\mathbf{r}} \chi_\sigma \tag{B.9}$$

in volume ν. We rewrite the Hamiltonian as:

$$H_{e,e} = \frac{1}{2} \sum_{\mathbf{k}_i, \sigma_i} < \mathbf{k}_1\sigma_1, \mathbf{k}_2\sigma_2 \mid \frac{e^2}{\mid \mathbf{r_i} - \mathbf{r_j} \mid} \mid \mathbf{k}_4\sigma_4, \mathbf{k}_3\sigma_3 > c_{\mathbf{k}_1\sigma_1}^\dagger c_{\mathbf{k}_2\sigma_2}^\dagger c_{\mathbf{k}_3\sigma_3} c_{\mathbf{k}_4\sigma_4} \tag{B.10}$$

The overlap matrix is given by:

$$
\begin{aligned}
< \mathbf{k}_1\sigma_1, \mathbf{k}_2\sigma_2 \mid \frac{e^2}{\mid \mathbf{r_i} - \mathbf{r_j} \mid} \mid \mathbf{k}_4\sigma_4, \mathbf{k}_3\sigma_3 > \quad &= \quad \int d^3\mathbf{r} \int d^3\mathbf{r}' \frac{1}{\sqrt{\nu}} \exp^{-i\mathbf{k}_1\cdot\mathbf{r}} \frac{1}{\sqrt{\nu}} \exp^{-i\mathbf{k}_2\cdot\mathbf{r}} \\
&\cdot \quad \frac{e^2}{\mid \mathbf{r_i} - \mathbf{r_j} \mid} \frac{1}{\sqrt{\nu}} \exp^{i\mathbf{k}_4\cdot\mathbf{r}} \frac{1}{\sqrt{\nu}} \exp^{i\mathbf{k}_3\cdot\mathbf{r}} \delta_{\sigma_1\sigma_4}\delta_{\sigma_2\sigma_3} \\
&= \quad \frac{\delta_{\sigma_1\sigma_4}\delta_{\sigma_2\sigma_3}}{V}\delta(\mathbf{k}_1 + \mathbf{k}_2 - \mathbf{k}_3 - \mathbf{k}_4)
\end{aligned}
\tag{B.11}
$$

And, therefore, considering the moment conservation of the interaction, we have:

$$
H_{e,e} = \frac{e^2}{2} \sum_{\mathbf{k},\mathbf{k}',\mathbf{q},\sigma,\sigma'} c^{\dagger}_{(\mathbf{k}+\mathbf{q})\sigma} c^{\dagger}_{(\mathbf{k}'-\mathbf{q})\sigma'} \frac{1}{q^2} c_{\mathbf{k}'\sigma'} c_{\mathbf{k}\sigma} \tag{B.12}
$$

This is the Hamiltonian form of Coulombian interaction energy.

Appendix C

Mean Field Theory.

The effect of many-body in the study of particle interaction in general is complicated by the terms of correlation in electron-electron interaction. And, to facilitate the approach of physical methods, a good model for average particle density is commonly used. The medium field model.

In the image below [61] we see on the left a physical system of the interaction of particles and on the right the interactions are replaced by an average density. Fact that directly affects the Hamiltonian of electron-electron interaction. So, a Hamiltonian model of two fluids described by operators a_ν and b_ν, is:

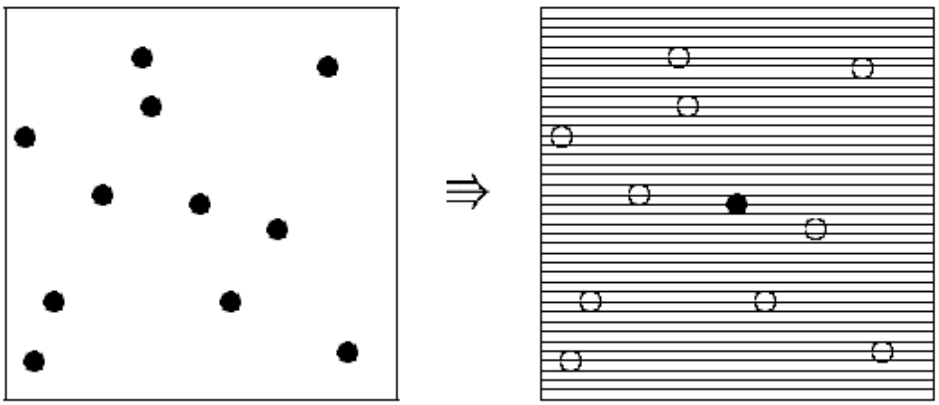

Figure C.1: Illustration of the mean field idea. Left box shows the interaction between the particle. To the right are the interactions experienced by the black particle replaced by an average interaction due a mean density.

$$H = \sum_{\nu} n_\nu^a a_\nu^\dagger a_\nu + \sum_{\mu} n_\mu^b b_\mu^\dagger b_\mu + \sum_{\mu\mu',\nu\nu'} V_{\mu\mu',\nu\nu'} a_\nu^\dagger b_\mu^\dagger b_{\mu'} a_{\nu'} \tag{C.1}$$

where n_ν^a and n_μ^b represent the particle densities followed by the density and $V_{\mu\mu',\nu\nu'}$ the energy of interaction. For a deviation of the density operators from their average values, it is defined as

$$A_{\nu\nu'} = a_\nu^\dagger a_\nu - < a_\nu^\dagger a_\nu > \tag{C.2}$$

and

$$B_{\nu\nu'} = b^\dagger_\nu b_\nu - < b^\dagger_\nu b_\nu > \tag{C.3}$$

Then we have:

$$\begin{aligned} H &= \sum_\nu n^a_\nu a^\dagger_\nu a_\nu + \sum_\mu n^b_\mu b^\dagger_\mu b_\mu \\ &+ \sum_{\mu\mu',\nu\nu'} V_{\mu\mu',\nu\nu'}(a^\dagger_\nu a_\nu < b^\dagger_\nu b_\nu > + b^\dagger_\mu b_\mu < a^\dagger_\nu a_\nu >) \\ &+ -\sum_{\mu\mu',\nu\nu'} V_{\mu\mu',\nu\nu'} < a^\dagger_\nu a_\nu >< b^\dagger_\nu b_\nu > \end{aligned} \tag{C.4}$$

This allows the interaction energy to be rewritten in terms of average densities and reduces the order of operators by simplifying the Hamiltonian.